IEEE Access
Multidisciplinary | Rapid Review | Open Access Journal

IEEE ELECTRONICS PACKAGING SOCIETY SECTION

Received December 23, 2021, accepted January 13, 2022, date of publication January 27, 2022, date of current version February 11, 2022.

Digital Object Identifier 10.1109/ACCESS.2022.3147034

Data-Driven Extraction of Uniformly Stable and Passive Parameterized Macromodels

TOMMASO BRADDE, (Member, IEEE), STEFANO GRIVET-TALOCIA, (Fellow, IEEE), ALESSANDRO ZANCO, (Member, IEEE), AND GIUSEPPE C. CALAFIORE, (Fellow, IEEE)
Department of Electronics and Telecommunications, Politecnico di Torino, 10129 Torino, Italy
Corresponding author: Tommaso Bradde (tommaso.bradde@polito.it)

ABSTRACT A robust algorithm for the extraction of reduced-order behavioral models from sampled frequency responses is proposed. The system under investigation can be any Linear and Time Invariant structure, although the main emphasis is on devices that are relevant for Signal and Power Integrity and RF design, such as electrical interconnects and integrated passive components. We assume that the device under modeling is parameterized by one or more design variables, which can be related to geometry or materials. Therefore, we seek for multivariate macromodels that reproduce the dynamic behavior over a predefined frequency band, with an explicit embedded dependence of the model equations on these external parameters. Such parameterized macromodels may be used to construct component libraries and prove very useful in fast system-level numerical simulations in time or frequency domain, including optimization, what-if, and sensitivity analysis. The main novel contribution is the formulation of a finite set of convex constraints that are applied during model identification, which provide sufficient conditions for uniform model stability and passivity throughout the parameter space. Such constraints are characterized by an explicit control allowing for a trade-off between model accuracy and runtime, thanks to some special properties of Bernstein polynomials. In summary, we propose a method to systematically address the longstanding problem of multivariate stability and passivity enforcement in data-driven model order reduction, which insofar has been tackled only via either over-conservative or heuristic and possibly unreliable methods.

INDEX TERMS Passive macromodeling, reduced-order modeling, parameterized modeling, data-driven model order reduction, Bernstein polynomials, linear matrix inequalities.

I. INTRODUCTION

Mathematical modeling is a cornerstone for modern technological advancement and industrial manufacturing. The possibility of accurately predicting the behavior of a given design allows engineers to perform preliminary testing and verification stages without relying on the construction of physical prototypes, which is highly consuming in terms of strategical assets. In this view, the industrial interest for mathematical models is moved not only by their effectiveness in predicting physical phenomena, but also by their potential for saving resources in terms of manpower and time-to-market.

For this reason, reduced order models or ''macromodels'' gained an increasing importance in the field of Computer Aided Design. The rationale behind such models is to predict the behavior of a given system with minimal computational efforts, by accurately reproducing those physical quantities that are of interest within a specific simulation, i.e. the required system outputs [1]–[3]. The intrinsic complexity of the first-principle physical laws (e.g. Maxwell's equations) is reduced to a small set of explanatory instrumental variables that are sufficient to predict the input-output relationship of interest. In particular, in the field of electronics manufacturing, the enormous complexity of state-of-the-art devices is such that behavioral models find major room for practical exploitation, in particular when dealing with passive electromagnetic devices [4]–[6] such as electrical interconnects and integrated components.

The generation of a macromodel is usually performed by following a well established workflow. A physical model for the device is first instantiated within a CAD environment able to provide a highly detailed description of the structure based on the Maxwell's equations. Once the interface electrical

The associate editor coordinating the review of this manuscript and approving it for publication was Ravi Mahajan.

ports are defined, a finite-bandwidth characterization of the system is obtained in terms of samples associated with a specified network function, typically in the scattering representation. A rational fitting process [7]–[10] is then performed over this available data in order to obtain a closed form expression which best explains the associated input-output behavior. The resulting rational model of the network function is then synthesized into an equivalent and low-complexity SPICE netlist, that can be exploited to perform fast numerical simulations at the system level.

The above procedure can be extended by requiring that the macromodel mimics the behavior of the structure for different configurations of a set of design or physical parameters, whose value is not fixed a priori but is known to belong to a prescribed set. In such a case, the network function data are sampled in correspondence of a finite number of parameters configurations, and a multivariate modeling strategy is pursued to obtain a parameterized macromodel that can replace the original structure for all of the parameters configurations of interest [11]–[15].

When the macromodel is to be used within system-level simulations, it is crucial that the associated equivalent circuit preserves some fundamental structural properties of the true device. In particular, passive components and interconnects, which are unable to generate energy on their own, must be represented by certified passive macromodels [6], [16]. Otherwise, the models can be the root cause of spurious instabilities, thus impairing the entire modeling and simulation workflow.

While the generation of passive univariate (non-parameterized) macromodels can mostly be considered as a solved problem [17]–[19], this is not true for the more complex parameterized case, and the topic is still subject of active research. Many different approaches have been proposed in the literature to tackle the passive parameterized macromodeling problem, but an ultimate fast, efficient and robust methodology is still not available.

Among the available strategies, some [11], [12], [20], [21] rely on passivity-preserving interpolation schemes. These approaches aim at building multivariate macromodels by interpolating a set of ''root'' univariate macromodels constructed at several discrete parameter instances. In case the root models are passive, the use of passivity preserving interpolation schemes guarantees the uniform passivity of the resulting multivariate model. The simplicity of these approaches comes with some serious drawbacks. For instance, the resulting multivariate model may show nonphysical augmented complexity and/or incorrect model behavior for parameter combinations that are different from the training samples.

Other techniques waive these structural passivity preserving properties in favor of more compact parameterized macromodels, which are identified through a well-established multivariate rational fitting procedure [14]. Uniform stability can be enforced by embedding some constraints in the fitting process. These constraints can be either based on (adaptive) sampling in the parameter space [22], [23], or by imposing some sign properties in the model coefficients [24]. The former approach may miss small stability violations due to the finite number of constraints that can be constructed, while the latter is known to be over-conservative and may lead to a model with reduced accuracy. In this framework, passivity enforcement is usually performed by post-processing, so that the model is iteratively perturbed until all the passivity violations are removed [25]. Two main problems affect this strategy: first, identification of passivity violations in a multivariate setting requires sampling, so that it is possible that some passivity violations are not identified and thus not removed; second, removal of a passivity violation requires the solution of a nonlinear optimization problem, whose linearization during iterations may lead to further loss of accuracy and possibly lack of convergence.

This work proposes a novel constrained multivariate rational fitting framework, that overcomes all above limitations and drawbacks. The approach can be summarized as follows.

1) The model structure is defined as a ratio between a matrix numerator and a scalar denominator, which are both expanded into a partial fraction basis (with stable basis poles) along frequency and multivariate Bernstein polynomials in the parameter space.
2) Stability conditions along frequency are expressed as a (continuously) parameterized Kalman-Yakubovick-Popov (KYP) linear matrix inequality, which depends only on the model denominator.
3) A finite number of convex constraints providing a *sufficient condition* for uniform stability is derived by expanding all terms of the above KYP condition in terms of Bernstein polynomials, and by exploiting some unique properties of such polynomials.
4) Passivity conditions along frequency are expressed as a parameterized KYP (similarly to point 2 above), which depends only on the model numerator.
5) A finite number of convex constraints providing a *sufficient condition* for uniform passivity is derived as in point 3, through a Bernstein polynomial expansion of the above KYP formulation.
6) The conservativity introduced by the discretization in points 3 and 5 is reduced by exploiting a special degree elevation property of Bernstein polynomials.

In the above list, points 1, 2 and 4 are reformulations of known results. Preliminary ideas based on point 5 have been recently published in [26] for parameterized macromodels including a single external parameter; expanding on such preliminary ideas, we present a full treatment of the theoretical derivations that legitimate the validity of points 3 and 5 when generating macromodels that include an arbitrary number of external parameters; the practical effectiveness of the proposed approach is further enhanced by introducing the conservativity reduction strategy of point 6.

We remark that the effectiveness of the constraints discretization strategy based on Bernstein polynomials involved

in points 3 and 5 has been also recently discussed in [27] in a more general setting.

From the computational standpoint, the proposed method consists of

- an iterative low-complexity least squares identification of the denominator of the model, where special Linear Matrix Inequality (LMI) constraints are used to enforce uniform stability;
- a single higher-complexity LMI-constrained least squares problem for the identification of the numerator (matrix) coefficients, which guarantees uniform model passivity.

The resulting algorithm is thus fully deterministic and robust, since it does not rely on sampling and is based on a convex formulation which is solved in finite time using standard optimization software.

The proposed approach has a single main limitation, in terms of the overall complexity of the models that can be processed. The scalability analysis and the numerical examples that follow show that only small and medium-scale models are tractable, thus providing an applicability limit of proposed framework. This limit is in fact common to all applications that are based on LMI constraints, not only in model order reduction but also in the more general field of modern control system engineering and numerical linear algebra.

This paper is organized as follows. Section II introduces some notation and general facts, considered as preliminaries and background. Section III states the main considered problem, defines the adopted model structure, and recalls the existing model identification methods; also this section is to be regarded as background material. Sections IV and V provide a complete derivation of proposed uniform stability and passivity conditions, respectively. Together with Sec. VI dedicated to the reduction of conservativity, they form the key novel material of this work. Section VII presents a set of numerical results together with discussion on performance and assessment of applicability limits. Conclusions are finally drawn in section VIII.

II. PRELIMINARIES AND NOTATION

In the following, we denote with $\mathbb{N}$, $\mathbb{R}$, and $\mathbb{C}$, the fields of natural, real and complex numbers, respectively. The symbol s is reserved for the Laplace variable, and $j = \sqrt{-1}$ is the imaginary unit. Scalars are denoted with a plain lowercase font x, while uppercase fonts denote matrices X, whose size is specified if not clear from the context. Matrix transpose and Hermitian transpose are denoted with $X^\top$ and $X^\star$, respectively. The set of symmetric matrices of size n is denoted as $\mathbb{S}_n$; accordingly, $\mathbb{S}_n^-$ denotes the cone of negative semi-definite matrices of size n. A given transfer function is denoted as $\mathsf{H}(s)$, and $\mathbb{I}_\mathrm{P}$ is reserved for the identity matrix of size P.

We define a multi-index as a d-dimensional collection of indices $\boldsymbol{i} = (i_1, \ldots, i_d) \in \mathbb{N}^d$. Given two multi-indices $\boldsymbol{j}$ and $\boldsymbol{k}$, we write $\boldsymbol{j} \leq \boldsymbol{k}$ meaning $j_1 \leq k_1, \ldots, j_d \leq k_d$. The sum operation $\boldsymbol{j} + \boldsymbol{k}$ between two multi-indices returns a multi-index $\boldsymbol{i} = (j_1 + k_1, \ldots, j_d + k_d)$. The $\max(\boldsymbol{j}, \boldsymbol{k})$ [resp. $\min(\boldsymbol{j}, \boldsymbol{k})$] function returns the component-wise maximum (resp. minimum) for each entry of its arguments. In this context, we also define the multi-index binomial coefficient

$$\binom{\boldsymbol{j}}{\boldsymbol{k}} = \prod_{i=1}^{d} \binom{j_i}{k_i}. \tag{1}$$

Let $p(\boldsymbol{\vartheta}) : \mathbb{R}^d \to \mathbb{R}$ be a generic multivariate polynomial in d variables $\boldsymbol{\vartheta} = (\vartheta_1 \ldots, \vartheta_d)$. In particular, we make extensive use of Bernstein polynomials. For $d = 1$,

$$b_\ell^{\bar{\ell}}(\vartheta) = \binom{\bar{\ell}}{\ell} \vartheta^\ell (1-\vartheta)^{\bar{\ell}-\ell}, \quad \ell = 0, \ldots, \bar{\ell} \tag{2}$$

defines the ℓ-th Bernstein polynomial of degree $\bar{\ell}$ in the scalar variable ϑ. For $d > 1$, the $\boldsymbol{\ell}$-th multivariate Bernstein polynomial of multi-degree $\bar{\boldsymbol{\ell}}$ is defined as

$$b_{\boldsymbol{\ell}}^{\bar{\boldsymbol{\ell}}}(\boldsymbol{\vartheta}) = b_{\ell_1}^{\bar{\ell}_1}(\vartheta_1) \times \cdots \times b_{\ell_d}^{\bar{\ell}_d}(\vartheta_d) \tag{3}$$

where

$$\bar{\boldsymbol{\ell}} = (\bar{\ell}_1, \ldots, \bar{\ell}_d) \tag{4}$$

is the multi-index collecting the degrees of the polynomials in each individual variable ϑ_k. For a given set of maximum degrees $\bar{\boldsymbol{\ell}}$, we define the associated set of admissible indices as

$$\mathcal{I}_{\bar{\boldsymbol{\ell}}} = \{\boldsymbol{\ell} \in \mathbb{N}^d : \boldsymbol{\ell} \leq \bar{\boldsymbol{\ell}}\}. \tag{5}$$

For any multivariate polynomial matrix function in the Bernstein basis

$$F(\boldsymbol{\vartheta}) : \mathbb{R}^d \to \mathbb{R}^{m \times n} = \sum_{\boldsymbol{\ell} \in \mathcal{I}_{\bar{\boldsymbol{\ell}}}} F^{\boldsymbol{\ell}}\, b_{\boldsymbol{\ell}}^{\bar{\boldsymbol{\ell}}}(\boldsymbol{\vartheta}) \tag{6}$$

we denote as *control points* the elements of the set $\{F^{\boldsymbol{\ell}} : \boldsymbol{\ell} \in \mathcal{I}_{\bar{\boldsymbol{\ell}}}\}$, in short $\{F^{\boldsymbol{\ell}}\}$.

We will exploit some notable properties of multivariate Bernstein polynomials, which we report here following [28]. First, we recall that such polynomials are non-negative and provide a partition of unity for any generic dimension d and maximum degree $\bar{\boldsymbol{\ell}}$

$$b_{\boldsymbol{\ell}}^{\bar{\boldsymbol{\ell}}}(\boldsymbol{\vartheta}) \geq 0 \quad \forall \boldsymbol{\ell} \in \mathcal{I}_{\bar{\boldsymbol{\ell}}}, \quad \sum_{\boldsymbol{\ell} \in \mathcal{I}_{\bar{\boldsymbol{\ell}}}} b_{\boldsymbol{\ell}}^{\bar{\boldsymbol{\ell}}}(\boldsymbol{\vartheta}) = 1, \quad \forall \boldsymbol{\vartheta} \in \Theta. \tag{7}$$

These two properties imply that all the values attained by functions (6) are obtained via a convex combination of the control points $\{F^{\boldsymbol{\ell}}\}$.

A multivariate Bernstein polynomial of degree $\bar{\boldsymbol{\ell}}$ can be equivalently rewritten in terms of another Bernstein polynomial of higher degree, exploiting the so-called *degree elevation* property. Consider a Bernstein polynomial $p(\boldsymbol{\vartheta})$ of degree $\bar{\boldsymbol{\ell}}$ and a degree increment $\boldsymbol{e} = (e_1, \ldots, e_2) \geq 0$. Then, $p(\boldsymbol{\vartheta})$ admits the two following equivalent representations

$$p(\boldsymbol{\vartheta}) = \sum_{\boldsymbol{\ell} \in \mathcal{I}_{\bar{\boldsymbol{\ell}}}} p^{\boldsymbol{\ell}}\, b_{\boldsymbol{\ell}}^{\bar{\boldsymbol{\ell}}}(\boldsymbol{\vartheta}) = \sum_{\boldsymbol{\gamma} \in \mathcal{I}_{\bar{\boldsymbol{\gamma}}}} g^{\boldsymbol{\gamma}}\, b_{\boldsymbol{\gamma}}^{\bar{\boldsymbol{\gamma}}}(\boldsymbol{\vartheta}), \quad \bar{\boldsymbol{\gamma}} = \bar{\boldsymbol{\ell}} + \boldsymbol{e} \tag{8}$$

where the set of coefficients $g^{\boldsymbol{\gamma}}$ are obtained as convex combinations of the original coefficients $p^{\boldsymbol{\ell}}$

$$g^{\boldsymbol{\gamma}} = \sum_{\boldsymbol{s}\in\mathcal{S}} \frac{\binom{\bar{\boldsymbol{\ell}}}{\boldsymbol{s}}\binom{\boldsymbol{e}}{\boldsymbol{\gamma}-\boldsymbol{s}}}{\binom{\bar{\boldsymbol{\ell}}+\boldsymbol{e}}{\boldsymbol{\gamma}}} p^{\boldsymbol{s}}, \quad \boldsymbol{\gamma}\in\mathcal{I}_{\bar{\boldsymbol{\gamma}}}, \tag{9}$$

where the sum is performed over the set of multi-indices $\mathcal{S} = \{\boldsymbol{s} : \boldsymbol{s} = \max(\boldsymbol{0}, \boldsymbol{\gamma}-\boldsymbol{e}), \ldots, \min(\bar{\boldsymbol{\ell}}, \boldsymbol{\gamma})\}$. Finally, given two Bernstein polynomials $p(\boldsymbol{\vartheta})$, $g(\boldsymbol{\vartheta})$ having total degree $\bar{\boldsymbol{\ell}}$ and $\bar{\boldsymbol{\gamma}}$ respectively, their product $h(\boldsymbol{\vartheta})$ can be expressed as a polynomial of total degree $\bar{\boldsymbol{\beta}} = \bar{\boldsymbol{\ell}} + \bar{\boldsymbol{\gamma}}$, whose coefficients $h^{\boldsymbol{\beta}}$ are

$$h^{\boldsymbol{\beta}} = \sum_{\boldsymbol{s}\in\mathcal{S}} \frac{\binom{\bar{\boldsymbol{\ell}}}{\boldsymbol{s}}\binom{\bar{\boldsymbol{\gamma}}}{\boldsymbol{\beta}-\boldsymbol{s}}}{\binom{\bar{\boldsymbol{\ell}}+\bar{\boldsymbol{\gamma}}}{\boldsymbol{\beta}}} p^{\boldsymbol{s}} g^{\boldsymbol{\beta}-\boldsymbol{s}}, \quad \boldsymbol{\beta}\in\mathcal{I}_{\bar{\boldsymbol{\beta}}} \tag{10}$$

where $\mathcal{S} = \{\boldsymbol{s} : \boldsymbol{s} = \max(\boldsymbol{0}, \boldsymbol{\beta}-\bar{\boldsymbol{\gamma}}), \ldots, \min(\bar{\boldsymbol{\ell}}, \boldsymbol{\beta})\}$.

III. PROBLEM SETTING

A. GENERAL SETTING

We consider a generic P-port Linear and Time-Invariant (LTI) system, whose behavior depends on d real-valued physical or design parameters. Without loss of generality, the parameter vector $\boldsymbol{\vartheta} = (\vartheta_1, \ldots, \vartheta_d)$ is assumed to belong to a normalized d-dimensional hypercube $\Theta = [0, 1]_1 \times \ldots \times [0, 1]_d$, called the design space. Denoting with $\mathsf{H}(s, \boldsymbol{\vartheta})$ the $\mathrm{P}\times\mathrm{P}$ transfer function of the system, we assume that a highly detailed first-principle model is available, which can be used to evaluate the system response through its frequency-domain samples over a finite bandwidth of interest and for any given combination of the design variables

$$\tilde{H}_{k,m} = \tilde{\mathsf{H}}(j\omega_k, \boldsymbol{\vartheta}_m), \quad k = 1, \ldots \bar{k}, \ m = 1, \ldots, \bar{m}. \tag{11}$$

Most commonly, such data samples are available as the scattering matrix of the reference device. When the structure under modeling is known to be passive, it is assumed that the data samples are compliant with the appropriate passivity conditions. It is also assumed that the available samples are sufficient to characterize the variations of the frequency responses over the target frequency band: indeed, any information that is not embedded in the input data cannot be reproduced by any model constructed using such data.

The goal of parameterized macromodeling is to synthesize a reduced-order rational model with a transfer function $\mathsf{H}(s, \boldsymbol{\vartheta})$ that matches the set of input training data

$$\mathsf{H}(j\omega_k, \boldsymbol{\vartheta}_m) \approx \tilde{H}_{k,m}, \quad k = 1, \ldots \bar{k}, \ m = 1, \ldots, \bar{m}. \tag{12}$$

The rational structure of the model allows for a straightforward conversion of the transfer function into a parameterized equivalent circuit of reduced order that can be exploited within off-the-shelf SPICE environments (not discussed here, see e.g. [6], [23]).

B. MODEL STRUCTURE

Consistently with most of the existing literature on this subject [14], [29], we assume the following *Parameterized-Sanathanan-Koerner (PSK)* model structure

$$\mathsf{H}(s, \boldsymbol{\vartheta}) = \frac{\mathsf{N}(s, \boldsymbol{\vartheta})}{\mathsf{D}(s, \boldsymbol{\vartheta})} = \frac{\sum_{i=0}^{\bar{n}} \sum_{\boldsymbol{\ell}\in\mathcal{I}_{\bar{\boldsymbol{\ell}}}} R_{i,\boldsymbol{\ell}}\, b_{\boldsymbol{\ell}}^{\bar{\boldsymbol{\ell}}}(\boldsymbol{\vartheta})\, \varphi_i(s)}{\sum_{i=0}^{\bar{n}} \sum_{\boldsymbol{\ell}\in\mathcal{I}_{\bar{\boldsymbol{\ell}}}} r_{i,\boldsymbol{\ell}}\, b_{\boldsymbol{\ell}}^{\bar{\boldsymbol{\ell}}}(\boldsymbol{\vartheta})\, \varphi_i(s)}, \tag{13}$$

where the basis functions $\varphi_i(s)$ are constructed from a set of predefined poles $\{q_1, \ldots, q_{\bar{n}}\}$ with $\Re\{q_i\} < 0\,\forall i$ as

$$\begin{cases} \varphi_i(s) = (s - q_i)^{-1}, & q_i \in \mathbb{R} \\ \varphi_i(s) = [(s - q_i)^{-1} + (s - q_i^\star)^{-1}] & q_i \in \mathbb{C} \\ \varphi_{i+1}(s) = j[(s - q_i)^{-1} - (s - q_i^\star)^{-1}] & q_{i+1} = q_i^\star \in \mathbb{C} \end{cases} \tag{14}$$

with $\varphi_0(s) = 1$. Therefore, both $\mathsf{N}(s, \boldsymbol{\vartheta})$ and $\mathsf{D}(s, \boldsymbol{\vartheta})$ are stable rational functions of the Laplace variable s, sharing the same set of poles. The Bernstein bases are exploited to parameterize $\mathsf{N}(s, \boldsymbol{\vartheta})$ and $\mathsf{D}(s, \boldsymbol{\vartheta})$ via the unknown model coefficients $r_{i,\boldsymbol{\ell}} \in \mathbb{R}$ and $R_{i,\boldsymbol{\ell}} \in \mathbb{R}^{\mathrm{P}\times\mathrm{P}}$. As these two transfer functions share the same set of common poles, the zeros and the poles of $\mathsf{H}(s, \boldsymbol{\vartheta})$ coincide with the zeros of $\mathsf{N}(s, \boldsymbol{\vartheta})$ and $\mathsf{D}(s, \boldsymbol{\vartheta})$ respectively. The PSK model structure (13) thus provides a parameterization of both zeros and poles of each individual model response. Note that the basis poles q_i cancel out in (13) and are not poles of the model. They are only instrumental for the definition of the barycentric basis functions $\varphi_i(s)$ upon which the model structure is constructed.

C. MODEL IDENTIFICATION

The model coefficients are found by minimizing the model-data error according to fitting condition (12), which is solved through a sequence of linear least squares problems based on the linearized approximation

$$\frac{\mathsf{N}^{\mu}(j\omega_k, \boldsymbol{\vartheta}_m) - \mathsf{D}^{\mu}(j\omega_k, \boldsymbol{\vartheta}_m)\tilde{H}_{k,m}}{\mathsf{D}^{\mu-1}(j\omega_k, \boldsymbol{\vartheta}_m)} \approx 0, \quad k = 1, \ldots \bar{k}, \quad m = 1, \ldots, \bar{m} \tag{15}$$

where $\mu = 1, 2, \ldots$ is the iteration index and $\mathsf{D}^{\mu-1}$ is known at each iteration μ since based on estimates of the denominator coefficients $r_{i,\boldsymbol{\ell}}$ at the previous iteration $\mu - 1$. The first iteration is initialized with $\mathsf{D}^0(j\omega, \boldsymbol{\vartheta}) = 1$. Condition (15) is equivalent to (12) whenever $\mathsf{D}^{\mu}(j\omega, \boldsymbol{\vartheta}) = \mathsf{D}^{\mu-1}(j\omega, \boldsymbol{\vartheta})$, which represents a convergence condition.

All the conditions (15) can be collected in a compact form

$$\begin{bmatrix} \Psi_x^{\mu} & \Psi_y^{\mu} \end{bmatrix} \begin{bmatrix} x^{\mu} \\ y^{\mu} \end{bmatrix} \approx 0 \tag{16}$$

where vectors x^{μ}, y^{μ} collect the numerator and denominator coefficients $R_{i,\boldsymbol{\ell}}$ and $r_{i,\boldsymbol{\ell}}$, respectively, and Ψ_x^{μ} and Ψ_y^{μ} are constant (iteration-dependent) regressor matrix blocks. System (16) is solved in least squares sense, suitably complemented by a non-triviality constraint to rule out the all-zero solution [30]. Due to the particular structure of the regression matrix entering problem (16), each iteration can

be split in two steps, which seek for x^μ and y^μ separately, in order to improve the algorithm efficiency. The first step finds y^μ by solving a reduced least-squares system of the form

$$\Gamma_y^\mu y^\mu \approx 0, \tag{17}$$

obtained by elimination of x^μ in (16) through a QR decomposition. Once y^μ is available (e.g. as the singular vector of Γ_y^μ associated to its least singular value), the following system

$$\Psi_x^\mu x^\mu \approx -\Psi_y^\mu y^\mu \tag{18}$$

is solved to find the numerator unknowns x^μ. See [31] for further details about the algorithmic aspects of this decoupling strategy.

Iterations are stopped when the denominator estimate stabilizes, i.e., when the following condition is met

$$\delta^\mu = \frac{\left\| y^\mu - y^{\mu-1} \right\|_2}{\|y^\mu\|_2} \leq \epsilon \tag{19}$$

being ϵ a given threshold. Alternatively, the iteration is stopped if a maximum prescribed iteration number is reached. Notice that convergence criterion (19) does not involve the numerator unknowns x^μ; therefore, the solution of (18) can be deferred to the last iteration, once (19) is met.

D. PROBLEM STATEMENT

The objective of this work is to guarantee that the parameterized model (13) is uniformly stable and possibly uniformly passive throughout the design space Θ. We will achieve this goal by modifying the model identification steps by adding a set of semi-definite constraints providing provable sufficient conditions for uniform stability and passivity. We anticipate that uniform stability is achieved by constraining only the denominator estimate (17) and provides a necessary prerequisite to uniform passivity. The latter is controlled by constraining all model coefficients.

Let us recall the general conditions for the uniform passivity of a generic parameter-dependent scattering or immittance LTI system in terms of its transfer matrix

1) $\mathsf{H}(s, \boldsymbol{\vartheta})$ regular for $\Re\{s\} > 0 \; \forall \boldsymbol{\vartheta} \in \Theta$
2) $\mathsf{H}^*(s, \boldsymbol{\vartheta}) = \mathsf{H}(s^*, \boldsymbol{\vartheta}) \; \forall s \in \mathbb{C}, \; \forall \boldsymbol{\vartheta} \in \Theta$
3) $\Phi(s, \boldsymbol{\vartheta}) \succeq 0$ for $\Re\{s\} > 0, \; \forall \boldsymbol{\vartheta} \in \Theta$

where * denotes the complex conjugate, and

$$\Phi(s, \boldsymbol{\vartheta}) = \begin{cases} \mathbb{I}_\mathrm{P} - \mathsf{H}^\star(s, \boldsymbol{\vartheta})\mathsf{H}(s, \boldsymbol{\vartheta}) & \text{scattering,} \\ \mathsf{H}^\star(s, \boldsymbol{\vartheta}) + \mathsf{H}(s, \boldsymbol{\vartheta}) & \text{immittance.} \end{cases} \tag{20}$$

Condition 1 is related to uniform stability, whereas the realness condition 2 is enforced by construction by adopted model structure (13). Condition 3 defines uniform dissipativity in terms of Bounded Realness (in the scattering case) and Positive Realness (in the immittance case). Wihtout loss of generality, we will only consider the Bounded Realness conditions in the following, since Positive Realness can be achieved with a straightforward adaptation.

In summary, we will propose a solution to the following two problems:

Problem 1: Derive a numerically viable approach to estimate the model coefficients $r_{i,\boldsymbol{\ell}}$, so that Condition 1 is fulfilled (*uniform stability*)

Problem 2: Assuming uniform stability, derive a numerically viable approach to estimate the model coefficients $R_{i,\boldsymbol{\ell}}$, so that Condition 3 is fulfilled (*uniform passivity*).

The solution of these two problems requires a set of state-space realizations for both model numerator and denominator, seen as individual transfer functions, which are introduced next.

E. STATE-SPACE REALIZATIONS

A state-space realization for the denominator transfer function can be constructed as follows [14]

$$\mathsf{D}(s, \boldsymbol{\vartheta}) \leftrightarrow \Sigma_\mathsf{D} = \left(\begin{array}{c|c} A_1 & B_1 \\ \hline C_1(\boldsymbol{\vartheta}) & D_1(\boldsymbol{\vartheta}) \end{array} \right), \tag{21}$$

where the constant matrices A_1, B_1 are

$$A_1 = \mathrm{blkdiag}\{A_{1,i}\} \in \mathbb{R}^{\bar{n} \times \bar{n}} \tag{22}$$

$$B_1 = [\ldots, B_{1,i}, \ldots]^\top \in \mathbb{R}^{\bar{n}}, \tag{23}$$

with

$$A_{1,i} = \begin{cases} q_i, & q_i \in \mathbb{R} \\ \begin{bmatrix} \sigma_i & \omega_i \\ -\omega_i & \sigma_i \end{bmatrix}, & q_i = \sigma_i \pm j\omega_i \in \mathbb{C} \end{cases} \tag{24}$$

$$B_{1,i} = \begin{cases} 1, & q_i \in \mathbb{R} \\ \begin{bmatrix} 2 & 0 \end{bmatrix}, & q_i = \sigma_i \pm j\omega_i \in \mathbb{C} \end{cases} \tag{25}$$

Note that, by construction, the pair (A_1, B_1) is controllable and A_1 is Hurwitz, as $\Re\{q_i\} < 0 \; \forall i$. The parameterized output matrices are available as Bernstein polynomials and read

$$C_1(\boldsymbol{\vartheta}) = \sum_{\boldsymbol{\ell} \in \mathcal{I}_{\bar{\ell}}} C_1^{\boldsymbol{\ell}} \, b_{\boldsymbol{\ell}}^{\bar{\ell}}(\boldsymbol{\vartheta}), \quad C_1^{\boldsymbol{\ell}} = [r_{1,\boldsymbol{\ell}}, \ldots, r_{\bar{n},\boldsymbol{\ell}}] \in \mathbb{R}^{1 \times \bar{n}} \tag{26}$$

$$D_1(\boldsymbol{\vartheta}) = \sum_{\boldsymbol{\ell} \in \mathcal{I}_{\bar{\ell}}} D_1^{\boldsymbol{\ell}} \, b_{\boldsymbol{\ell}}^{\bar{\ell}}(\boldsymbol{\vartheta}), \quad D_1^{\boldsymbol{\ell}} = r_{0,\boldsymbol{\ell}} \in \mathbb{R}. \tag{27}$$

Using a similar construction, we can realize the numerator transfer function as follows

$$\mathsf{N}(s, \boldsymbol{\vartheta}) \leftrightarrow \Sigma_\mathsf{N} = \left(\begin{array}{c|c} A & B \\ \hline C_2(\boldsymbol{\vartheta}) & D_2(\boldsymbol{\vartheta}) \end{array} \right) \tag{28}$$

where $A = \mathbb{I}_\mathrm{P} \otimes A_1$ and $B = \mathbb{I}_\mathrm{P} \otimes B_1$ with $\otimes$ denoting the matrix Kronecker product, and where

$$C_2(\boldsymbol{\vartheta}) = \sum_{\boldsymbol{\ell} \in \mathcal{I}_{\bar{\ell}}} C_2^{\boldsymbol{\ell}} \, b_{\boldsymbol{\ell}}^{\bar{\ell}}(\boldsymbol{\vartheta}) \quad C_2^{\boldsymbol{\ell}} \in \mathbb{R}^{\mathrm{P} \times \bar{n}\mathrm{P}}, \tag{29}$$

$$D_2(\boldsymbol{\vartheta}) = \sum_{\boldsymbol{\ell} \in \mathcal{I}_{\bar{\ell}}} D_2^{\boldsymbol{\ell}} \, b_{\boldsymbol{\ell}}^{\bar{\ell}}(\boldsymbol{\vartheta}) \quad D_2^{\boldsymbol{\ell}} = R_{0,\boldsymbol{\ell}} \in \mathbb{R}^{\mathrm{P} \times \mathrm{P}}. \tag{30}$$

For fixed $\boldsymbol{\ell}$, matrix $C_2^{\boldsymbol{\ell}}$ collects the elements of the model coefficients $R_{i,\boldsymbol{\ell}}$, $i > 0$ with a compatible ordering. The pair (A, B) inherits the controllability property from (A_1, B_1). All of the eigenvalues of A are stable.

IV. UNIFORM STABILITY CONDITIONS

This section presents a solution for Problem 1 and derives a set of algebraic and convex constraints providing a guaranteed uniform stability of the model.

Given the adopted model structure (13), stability is attained by constraining all the zeros of the denominator $\mathsf{D}(s, \boldsymbol{\vartheta})$ to have a negative real part, since these zeros coincide with the parameter-dependent model poles. The denominator $\mathsf{D}(s, \boldsymbol{\vartheta})$ satisfies by construction Conditions 1, 2 of Sec. III-D being a real rational and strictly stable function. If we are able to additionally enforce the dissipativity Condition 3, then $\mathsf{D}(s, \boldsymbol{\vartheta})$ becomes a certified uniformly Positive Real function. Since any Positive Real function is also minimum phase [32] with stable zeros, we conclude that enforcing (31) guarantees indirectly the uniform stability of the model $\mathsf{H}(s, \boldsymbol{\vartheta})$. Note that, under the working assumptions, Condition 3 can be replaced by the simpler condition

$$\mathsf{D}^{\star}(j\omega, \boldsymbol{\vartheta}) + \mathsf{D}(j\omega, \boldsymbol{\vartheta}) \geq 0 \quad \forall \boldsymbol{\vartheta} \in \Theta, \ \forall \omega, \tag{31}$$

since $\mathsf{D}(s, \boldsymbol{\vartheta})$ is strictly stable and bounded for $s \to \infty$, without poles on the imaginary axis $s = j\omega$.

This consideration has been extensively exploited in the literature to generate stable parameterized macromodels. From the numerical standpoint, (31) cannot be enforced directly, as it embeds an infinite number of constraints that must be verified over the entire continuous frequency-parameter space. Its enforcement has been addressed either by discretization into a finite set via sampling-based strategies [23], or by deriving over-conservative sufficient conditions on the sign of individual terms in the denominator expansion [24]. These two strategies are complementary from the point of view of the modeling performances: while the former guarantees high level of accuracy but does not provide a theoretical guarantee for uniform stability, the latter leads to provable stability and is very efficient but can result in accuracy degradation due to the approximate nature of the applied constraints. In what follows, we propose a scheme that retains the advantages of both approaches.

Let us consider the state-space realization (21) and define $Z_1(j\omega) = (j\omega\mathbb{I}_{\mathrm{P}} - A_1)^{-1}B_1$. Condition (31) can be rewritten as

$$Z_1(j\omega)^{\star} C_1(\boldsymbol{\vartheta})^{\top} + C_1(\boldsymbol{\vartheta}) Z_1(j\omega) + 2D_1(\boldsymbol{\vartheta}) \geq 0, \tag{32}$$

that must hold $\forall \boldsymbol{\vartheta} \in \Theta, \forall \omega$, or in the more compact matrix form

$$\begin{bmatrix} Z_1(j\omega) \\ \mathbb{I}_{\mathrm{P}} \end{bmatrix}^{\star} \begin{bmatrix} 0 & -C_1(\boldsymbol{\vartheta})^{\top} \\ -C_1(\boldsymbol{\vartheta}) & -2D_1(\boldsymbol{\vartheta}) \end{bmatrix} \begin{bmatrix} Z_1(j\omega) \\ \mathbb{I}_{\mathrm{P}} \end{bmatrix} \preceq 0. \tag{33}$$

Since the pair (A_1, B_1) is controllable, we can apply the Yakubovich lemma [33], [34] to cast this frequency domain inequality as the equivalent algebraic inequality

$$\forall \boldsymbol{\vartheta} \in \Theta, \quad \exists L(\boldsymbol{\vartheta}) \in \mathbb{S}_{\bar{n}} : \\ \Omega(A_1, B_1, L(\boldsymbol{\vartheta})) - \begin{bmatrix} 0 & C_1(\boldsymbol{\vartheta})^{\top} \\ C_1(\boldsymbol{\vartheta}) & 2D_1(\boldsymbol{\vartheta}) \end{bmatrix} \preceq 0, \tag{34}$$

where we define the auxiliary block matrix

$$\Omega(P, Q, R) = \begin{bmatrix} P^{\top}R + RP & RQ \\ Q^{\top}R & 0 \end{bmatrix} \tag{35}$$

for any triplet of matrices $P, Q, R = R^{\top}$ with compatible size, and where $L(\boldsymbol{\vartheta})$ plays the role of an energy storage function (Lyapunov matrix). Notice that (34) is a parameterized version of the well-established Positive Real Lemma [35], in which the additional requirement $L(\boldsymbol{\vartheta}) \succeq 0$ is automatically entailed by the fact that A_1 is Hurwitz.

Condition (34) is a robust Linear Matrix Inequality (LMI) condition on both the instrumental matrix $L(\boldsymbol{\vartheta})$ and the denominator coefficients $r_{i,\boldsymbol{\ell}}$, which enter the various matrix blocks according to (26)-(27). Although such conditions are convex, solving (17) for the denominator coefficients while enforcing (34) for all $\boldsymbol{\vartheta} \in \Theta$ is still a computationally intractable task. We have removed dependence on frequency, but a continuous dependence of the constraints in the parameters $\boldsymbol{\vartheta}$ remains.

This problem is addressed by restricting the class of the storage functions $L(\boldsymbol{\vartheta})$ to a finite-dimensional space. In particular, we adopt the following structure using an expansion into Bernstein polynomials

$$L(\boldsymbol{\vartheta}) = \sum_{\boldsymbol{\ell} \in \mathcal{I}_{\bar{\boldsymbol{\ell}}}} L^{\boldsymbol{\ell}} \, b_{\boldsymbol{\ell}}^{\bar{\boldsymbol{\ell}}}(\boldsymbol{\vartheta}), \quad L^{\boldsymbol{\ell}} \in \mathbb{S}_{\bar{n}} \ \forall \boldsymbol{\ell} \in \mathcal{I}_{\bar{\boldsymbol{\ell}}} \tag{36}$$

based on a set of unknown symmetric matrix coefficients $\{L^{\boldsymbol{\ell}}\}$. Using (36), (34) becomes

$$\forall \boldsymbol{\vartheta} \in \Theta, \quad \exists L^{\boldsymbol{\ell}} \in \mathbb{S}_{\bar{n}}, \ \boldsymbol{\ell} \in \mathcal{I}_{\bar{\boldsymbol{\ell}}} : \\ S(\boldsymbol{\vartheta}) = \sum_{\boldsymbol{\ell} \in \mathcal{I}_{\bar{\boldsymbol{\ell}}}} S^{\boldsymbol{\ell}} \, b_{\boldsymbol{\ell}}^{\bar{\boldsymbol{\ell}}}(\boldsymbol{\vartheta}) \preceq 0, \tag{37}$$

with

$$S^{\boldsymbol{\ell}} = \Omega(A_1, B_1, L^{\boldsymbol{\ell}}) - \begin{bmatrix} 0 & C_1^{\boldsymbol{\ell}\top} \\ C_1^{\boldsymbol{\ell}} & 2D_1^{\boldsymbol{\ell}} \end{bmatrix} \in \mathbb{S}_{\bar{n}+1}. \tag{38}$$

As all Bernstein polynomials are nonnegative, $b_{\boldsymbol{\ell}}^{\bar{\boldsymbol{\ell}}}(\boldsymbol{\vartheta}) \geq 0 \ \ \forall \boldsymbol{\ell} \in \mathcal{I}_{\bar{\boldsymbol{\ell}}}$, we see that (34) is implied by the following sufficient conditions

$$S^{\boldsymbol{\ell}} \preceq 0 \quad \forall \boldsymbol{\ell} \in \mathcal{I}_{\bar{\boldsymbol{\ell}}} \tag{39}$$

which can be exploited as a set of standard *non-parameterized* LMI constraints to be enforced during the estimation of the model denominator coefficients. More precisely, our proposed solution for uniform stability enforcement can be cast as the following semi-definite program

$$\min_{y^{\mu}} \left\| \Gamma^{\mu} y^{\mu} \right\|_2 \quad \text{s.t. } S^{\boldsymbol{\ell}} \preceq 0 \quad \forall \boldsymbol{\ell} \in \mathcal{I}_{\bar{\boldsymbol{\ell}}} \tag{40}$$

replacing the unconstrained least squares problem (17). The optimization problem (40) is a semi-definite program that can be solved through off-the-shelf convex optimization solvers.

Some remarks about the computational cost are in order. Let $\mathrm{Card}(\mathcal{I}_{\bar{\boldsymbol{\ell}}}) = V$. The solution of (40) involves

$(\bar{n}+1)V$ unknown model coefficients and $V((\bar{n}+1)^2+\bar{n}+1)/2$ instrumental variables. The size of the regressor matrix is $\Gamma^{\mu} \in \mathbb{R}^{\mathrm{P}^2 V\bar{n}\times V\bar{n}}$, as explained in [31]. The size of the symmetric matrices involved in the constraints is $\bar{n}+1$, and the number of matrix constraints is V. As one could expect, the proposed approach suffers from a curse of dimensionality when the dimension of the design space d increases, as both the number of denominator unknowns and the cardinality V of the admissible indices grows exponentially with d. However, as experimentally demonstrated in Section VII, the numerical solution of (40) requires affordable (desktop-level) computing resources when making use of state-of-the-art convex optimization solvers, at least for moderate dimension d (few units).

We conclude this section by noting that both (36) and (39) do introduce some amount of conservativity in the formulation with respect to the continuously parameterized form (34). We will show in Sec. VI that this amount can be effectively controlled and reduced thanks to the degree elevation property of the Bernstein polynomials.

V. UNIFORM PASSIVITY CONDITIONS

This section proposes a solution to the Problem 2 of Sec. IV, which aims at enforcing uniform dissipativity of the model. In the assumed scattering representation, this is equivalent to enforcing the model response $\mathsf{H}(s,\boldsymbol{\vartheta})$ to be Bounded Real throughout the design space Θ. As Bounded Realness requires as a prerequisite the uniform stability, we assume that the coefficients y^{μ} of the model denominator have already been identified by solving the convex program (40). Therefore, this section will focus on the identification of the coefficients x^{μ} of the model numerator, assuming as *frozen* the denominator coefficients.

Let us consider the non-expansivity Condition 3 of Sec. III-D, that we can equivalently restrict to the imaginary axis similarly to (31) as

$$\mathsf{H}^{\star}(j\omega,\boldsymbol{\vartheta})\mathsf{H}(j\omega,\boldsymbol{\vartheta}) \preceq \mathbb{I}_{\mathrm{P}} \quad \forall\omega\in\mathbb{R},\ \forall\boldsymbol{\vartheta}\in\Theta. \tag{41}$$

Exploiting the model structure (13) provides the equivalent form

$$\mathsf{N}^{\star}(j\omega,\boldsymbol{\vartheta})\mathsf{N}(j\omega,\boldsymbol{\vartheta}) - \mathbb{I}_{\mathrm{P}}\,\mathsf{D}^{\star}(j\omega,\boldsymbol{\vartheta})\mathsf{D}(j\omega,\boldsymbol{\vartheta}) \preceq 0, \quad \forall\omega\in\mathbb{R},\ \forall\boldsymbol{\vartheta}\in\Theta. \tag{42}$$

We now replace numerator and denominator with their state-space realization, as in Sec. IV. Before proceeding, we need to construct a Multi-Input Multi-Output (MIMO) realization of the auxiliary system $\mathbb{I}_{\mathrm{P}}\mathsf{D}(s,\boldsymbol{\vartheta})$ appearing in (42), which replicates the (scalar) denominator $\mathsf{D}(s,\boldsymbol{\vartheta})$ along the diagonal of a $\mathrm{P}\times\mathrm{P}$ matrix. This realization can be written as

$$\mathbb{I}_{\mathrm{P}}\mathsf{D}(s,\boldsymbol{\vartheta}) \leftrightarrow \left(\begin{array}{c|c} \mathbb{I}_{\mathrm{P}}\otimes A_1 & \mathbb{I}_{\mathrm{P}}\otimes B_1 \\ \hline \mathbb{I}_{\mathrm{P}}\otimes C_1(\boldsymbol{\vartheta}) & \mathbb{I}_{\mathrm{P}}\otimes D_1(\boldsymbol{\vartheta}) \end{array}\right) \tag{43}$$

$$= \left(\begin{array}{c|c} A & B \\ \hline C_{\otimes}(\boldsymbol{\vartheta}) & D_{\otimes}(\boldsymbol{\vartheta}) \end{array}\right), \tag{44}$$

where all state-space matrices are known since the denominator coefficients have already been determined. Note that the state matrices A and B are the same as for the numerator realization (28). Setting now $Z(j\omega) = (j\omega\mathbb{I}_{\bar{n}\mathrm{P}} - A)^{-1}B$ and using (43), (28), allows to cast condition (42) as

$$\begin{bmatrix} Z(j\omega) \\ \mathbb{I}_{\mathrm{P}} \end{bmatrix}^{\star} \Big(X_2(\boldsymbol{\vartheta}) - X_{\otimes}(\boldsymbol{\vartheta})\Big) \begin{bmatrix} Z(j\omega) \\ \mathbb{I}_{\mathrm{P}} \end{bmatrix} \preceq 0, \tag{45}$$

which must hold $\forall\boldsymbol{\vartheta}\in\Theta$ and $\forall\omega$, and where we have defined the auxiliary matrices

$$X_{\nu}(\boldsymbol{\vartheta}) = \begin{bmatrix} C_{\nu}^{\top}(\boldsymbol{\vartheta}) \\ D_{\nu}^{\top}(\boldsymbol{\vartheta}) \end{bmatrix} \begin{bmatrix} C_{\nu}(\boldsymbol{\vartheta}) & D_{\nu}(\boldsymbol{\vartheta}) \end{bmatrix}, \tag{46}$$

being the symbol ν a place-holder for the subscripts $\{2,\otimes\}$. As the pair (A,B) is controllable, the application of Yakubovich lemma [34] translates (45) into the following equivalent parameterized algebraic condition

$$\forall\boldsymbol{\vartheta}\in\Theta, \quad \exists P(\boldsymbol{\vartheta})\in\mathbb{S}_{\bar{n}P}: \quad X_2(\boldsymbol{\vartheta}) - X_{\otimes}(\boldsymbol{\vartheta}) + \Omega(A,B,P(\boldsymbol{\vartheta})) \preceq 0, \tag{47}$$

which can be interpreted as a reformulation of the classical Bounded Real lemma [35] for stable transfer functions which are parameterized according to the proposed model structure (13).

Condition (47) is similar to (34), with the additional complication that the numerator unknowns x^{μ} that are embedded in the parameterization of $C_2(\boldsymbol{\vartheta})$, $D_2(\boldsymbol{\vartheta})$ appear as quadratic terms in $X_2(\boldsymbol{\vartheta})$. It is nonetheless possible to reformulate (47) as a LMI. First, we write $X_{\otimes}(\boldsymbol{\vartheta})$ as a sum of Bernstein polynomials of total degree $\overline{\boldsymbol{m}} = 2\overline{\boldsymbol{\ell}}$

$$X_{\otimes}(\boldsymbol{\vartheta}) = \sum_{\boldsymbol{m}\in\mathcal{I}_{\overline{\boldsymbol{m}}}} X^{\boldsymbol{m}}\, b_{\boldsymbol{m}}^{\overline{\boldsymbol{m}}}(\boldsymbol{\vartheta}) \tag{48}$$

with symmetric matrix coefficients $X^{\boldsymbol{m}}$. Since the denominator coefficients $r_{i,\ell}$ are available, each $X^{\boldsymbol{m}}$ can be computed in closed form as the product of polynomials in Bernstein basis, using formula (10). Note that this expansion is exact. Second, we apply the inverse Schur complement to (47), obtaining the equivalent LMI condition

$$\left[\begin{array}{c|c} \Omega(A,B,P(\boldsymbol{\vartheta})) - X_{\otimes}(\boldsymbol{\vartheta}) & \begin{bmatrix} C_2(\boldsymbol{\vartheta}) & D_2(\boldsymbol{\vartheta}) \end{bmatrix}^{\top} \\ \hline \begin{bmatrix} C_2(\boldsymbol{\vartheta}) & D_2(\boldsymbol{\vartheta}) \end{bmatrix} & -\mathbb{I}_{\mathrm{P}} \end{array}\right] \preceq 0 \tag{49}$$

which must be verified $\forall\boldsymbol{\vartheta}\in\Theta$. Third, we apply the degree elevation property of Bernstein polynomials (8) to the off-diagonal blocks of (49). More precisely, we rewrite $C_2(\boldsymbol{\vartheta})$ and $D_2(\boldsymbol{\vartheta})$ as a sum of Bernstein polynomials of total degree $\overline{\boldsymbol{m}}$ starting from their original degree-$\overline{\boldsymbol{\ell}}$ expansions (29)-(30), and we cast the result in compact form as

$$Y(\boldsymbol{\vartheta}) = \sum_{\boldsymbol{m}\in\mathcal{I}_{\overline{\boldsymbol{m}}}} Y^{\boldsymbol{m}}\, b_{\boldsymbol{m}}^{\overline{\boldsymbol{m}}}(\boldsymbol{\vartheta}) = \sum_{\boldsymbol{\ell}\in\mathcal{I}_{\overline{\boldsymbol{\ell}}}} \begin{bmatrix} C_2^{\boldsymbol{\ell}\top} \\ D_2^{\boldsymbol{\ell}\top} \end{bmatrix} b_{\boldsymbol{\ell}}^{\overline{\boldsymbol{\ell}}}(\boldsymbol{\vartheta}). \tag{50}$$

The matrix coefficients $Y^{\boldsymbol{m}}$ depend linearly on the numerator coefficients $R_{i,\boldsymbol{\ell}}$. Fourth, we enforce the following structure for the instrumental matrix $P(\boldsymbol{\vartheta})$

$$P(\boldsymbol{\vartheta}) = \sum_{\boldsymbol{m}\in\mathcal{I}_{\overline{\boldsymbol{m}}}} P^{\boldsymbol{m}}\, b_{\boldsymbol{m}}^{\overline{\boldsymbol{m}}}(\boldsymbol{\vartheta}), \quad P^{\boldsymbol{m}}\in\mathbb{S}_{\bar{n}P}\ \ \forall\boldsymbol{m}\in\mathcal{I}_{\overline{\boldsymbol{m}}}. \tag{51}$$

Thanks to this assumption, all terms in (49) are Bernstein polynomials of total degree $\overline{\boldsymbol{m}}$, so that (49) can be rewritten in compact form using (50) and (51) as

$$F(\boldsymbol{\vartheta}) = \sum_{\boldsymbol{m}\in\mathcal{I}_{\overline{\boldsymbol{m}}}} F^{\boldsymbol{m}}\, b^{\overline{\boldsymbol{m}}}_{\boldsymbol{m}}(\boldsymbol{\vartheta}) \preceq 0 \quad \forall \boldsymbol{\vartheta}\in\Theta \tag{52}$$

with symmetric matrix coefficients

$$F^{\boldsymbol{m}} = \begin{bmatrix} \Omega(A,B,P^{\boldsymbol{m}}) - X^{\boldsymbol{m}} & Y^{\boldsymbol{m}} \\ Y^{\boldsymbol{m}\top} & -\mathbb{I}_{\mathrm{P}} \end{bmatrix} \in \mathbb{S}_g \tag{53}$$

of size $g = P\bar{n} + P$. Finally, since Bernstein polynomials are non-negative, we see that (49) is implied by the following set of semi-definite constraints

$$F^{\boldsymbol{m}} \preceq 0, \quad \forall \boldsymbol{m}\in\mathcal{I}_{\overline{\boldsymbol{m}}}. \tag{54}$$

The above conditions can be easily incorporated within the numerator estimation procedure expressed by (18). This unconstrained least squares system in the unknown variables x^{μ} is thus replaced by the following LMI-constrained convex program

$$\min_{x^{\mu}} \left\| \Psi^{\mu}_{x} x^{\mu} + \Psi^{\mu}_{y} y^{\mu} \right\|_2 \quad \text{s.t. } F^{\boldsymbol{m}} \preceq 0, \quad \forall \boldsymbol{m}\in\mathcal{I}_{\overline{\boldsymbol{m}}}. \tag{55}$$

The numerical solution (55) provides a set of numerator coefficients x^{μ} that guarantee uniform passivity of the model. Due to the convex formulation with a finite number of constraints, this solution is attained in polynomial time with standard convex optimization solvers. The data matrices $\Psi^{\mu}_{x,y}$ entering (55) have a row size depending on the amount of training data samples. If the passive structure under modeling is reciprocal, then the problem involves $M(\bar{n}+1)(\mathrm{P}^2/2 + \mathrm{P}/2)$ unknown model coefficients and $M(\mathrm{P}^2\bar{n}^2/2 + \mathrm{P}\bar{n}/2)$ instrumental variables, where $M = \mathrm{Card}(\mathcal{I}_{\overline{\boldsymbol{m}}})$. From these expressions we see that the complexity of the problem depends not only on the total number M of elements in the multivariate Bernstein basis used to represent the dissipativity constraints, but also on the number of interface ports P of the model. This implies that the proposed approach is only applicable to small-medium scale systems. This limitation is common to all convex formulations of passivity constraints based on the Positive and Bounded Real Lemmas.

As a final remark, we note that in our derivations we assumed the output matrices associated with the transfer functions $\mathsf{N}(s,\boldsymbol{\vartheta})$ and $\mathbb{I}_{\mathrm{P}}\mathsf{D}(s,\boldsymbol{\vartheta})$ to be expressed as Bernstein polynomials sharing the same total degree $\overline{\boldsymbol{\ell}}$. If one drops this assumption, the proposed derivations are still valid, as the elements of the matrix function (49) can always be represented as Bernstein polynomial series of equal degree, by exploiting the degree elevation property.

VI. DEGREE ELEVATION AND CONSERVATIVITY REDUCTION

The derivations of Sec. IV-V led to the pair of convex optimization problems (40) and (55) which, when solved in sequence, provide a guarantee of uniform stability and passivity of the parameterized model. All the derivations leading to the LMI constraints (39) and (54) are based on a chain of necessary and sufficient conditions, exception made for two main steps. First, the imposition of a particular polynomial structure for the instrumental matrices $L(\boldsymbol{\vartheta})$ and $P(\boldsymbol{\vartheta})$ may restrict the class of storage functions that may provide a stability or passivity certificate for the model. This in turn may restrict the class of models that can be obtained. In other words, these assumptions introduce some degree of conservativity in the identification process.

A second source of conservativity arises from the discretization of (37) into (39) and of (52) into (54). Considering the latter, the employed discretization is over-conservative because $F(\boldsymbol{\vartheta})$ may be uniformly negative semi-definite even in case some of the $F^{\boldsymbol{m}}$ are not. We now analyze this limitation in detail, and we propose an effective strategy to reduce the amount of conservativity, thereby improving the overall model accuracy.

We consider the replacement of (52) with the discretized set (54). Let $\mathcal{F}$ be the set spanned by all matrices $F(\boldsymbol{\vartheta})$ as $\boldsymbol{\vartheta}$ spans the design space Θ. By construction, this set is embedded in the convex hull generated by all matrix coefficients $F^{\boldsymbol{m}}$

$$\mathcal{F} = \{x : x = F(\boldsymbol{\vartheta}), \boldsymbol{\vartheta}\in\Theta\} \subseteq \mathrm{Conv}(\{F^{\boldsymbol{m}}\}). \tag{56}$$

Enforcing (54) guarantees uniform passivity by constraining all individual matrix coefficients $F^{\boldsymbol{m}}$ to be negative semi-definite, so that

$$F^{\boldsymbol{m}} \in \mathbb{S}_g^- \Rightarrow \mathrm{Conv}(\{F^{\boldsymbol{m}}\}) \subseteq \mathbb{S}_g^- \Rightarrow \mathcal{F} \subseteq \mathbb{S}_g^-. \tag{57}$$

The degree of conservativity depends on the distance between $\mathcal{F}$ and the boundary of $\mathrm{Conv}(\{F^{\boldsymbol{m}}\})$. The larger this distance, the larger the degree of conservativity in the passivity (stability) enforcement. Therefore, reduction of this distance will lead to a reduction of conservativity and to an improved model accuracy. Fortunately, the properties of Bernstein polynomials come at hand for this task, since it is well known that, for any matrix function in form (6), the set of control points (the matrix coefficients in the Bernstein expansion) converge uniformly to the value of the expanded function under repeated application of the degree elevation property [36]–[38]. This is graphically illustrated in Fig 1.

Let us apply this property to the present passivity (stability) enforcement case. We define $\boldsymbol{e} = \boldsymbol{m} + (e,\ldots,e)$. Then for any e we can always write

$$F(\boldsymbol{\vartheta}) = \sum_{\boldsymbol{m}\in\mathcal{I}_{\overline{\boldsymbol{m}}}} F^{\boldsymbol{m}}\, b^{\overline{\boldsymbol{m}}}_{\boldsymbol{m}}(\boldsymbol{\vartheta}) = \sum_{\boldsymbol{e}\in\mathcal{I}_{\overline{\boldsymbol{e}}}} F^{\boldsymbol{e}}\, b^{\overline{\boldsymbol{e}}}_{\boldsymbol{e}}(\boldsymbol{\vartheta}), \tag{58}$$

where the new control points $\{F^{\boldsymbol{e}}\}$ are obtained as convex combinations of $\{F^{\boldsymbol{m}}\}$ according to (9). We have

$$\mathcal{F} \subseteq \mathrm{Conv}(\{F^{\boldsymbol{e}}\}) \subseteq \mathrm{Conv}(\{F^{\boldsymbol{m}}\}), \quad \forall e\in\mathbb{N}. \tag{59}$$

For increasing e, we have the uniform convergence property [36]

$$\lim_{e\to\infty} \{F^{\boldsymbol{e}}\} = F(\boldsymbol{\vartheta}). \tag{60}$$

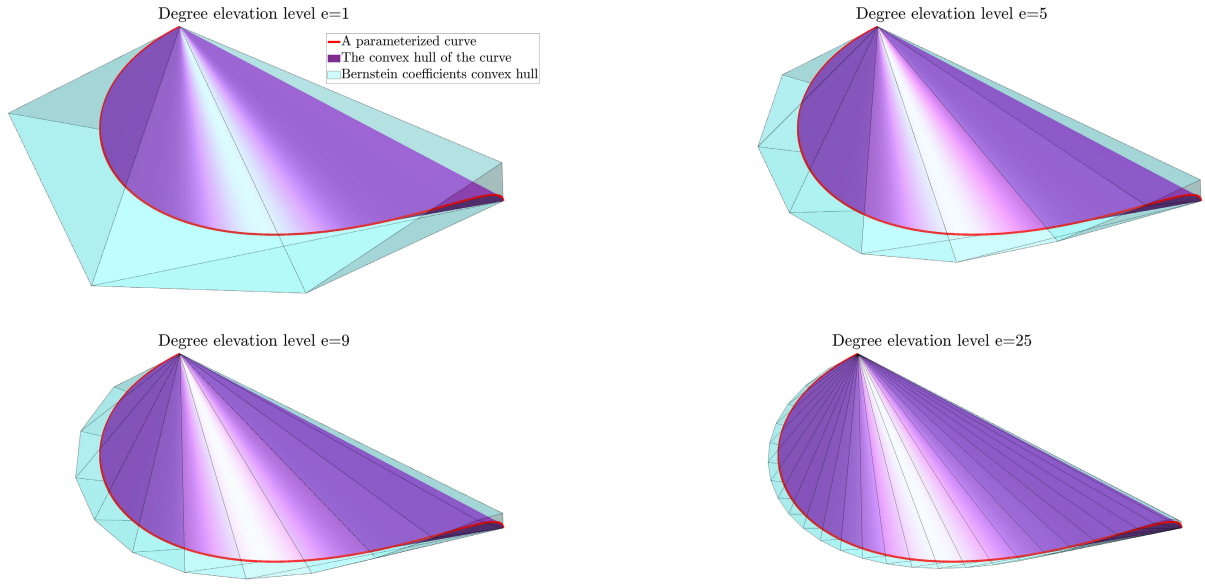

FIGURE 1. Graphical demonstration of the degree elevation effects. The red line represents the set $\mathcal{F}$ of the values attained by a function defined according to (6) for $d = 1$, $\bar{\ell} = 4$ and $F^{\ell} \in \mathbb{R}^3$; the purple volume is the convex hull of $\mathcal{F}$; the light blue polyhedra are the convex hulls of the control points $\{F^{\ell}\}$ for different levels of degree elevation. As the degree of the representation increases, the polyhedron approaches the underlying set $\mathcal{F}$, thus providing better and better outer approximations.

with a convergence rate $1/e$, see Fig. 1. For any given e, we can therefore replace (55) with a less conservative optimization problem

$$\min_{x^{\mu}} \left\| \Psi_x^{\mu} x^{\mu} + \Psi_y^{\mu} y^{\mu} \right\|_2 \quad \text{s.t. } F^{\boldsymbol{e}} \preceq 0, \quad \forall \boldsymbol{e} \in \mathcal{I}_{\bar{\boldsymbol{e}}} \tag{61}$$

where the constraint $F^{\boldsymbol{e}} \preceq 0$ becomes practically equivalent to (52) for sufficiently large e.

Switching to (61) does not modify the number of decision variables in the optimization. However, the number of LMI constraints increases reaching $E = \text{Card}(\mathcal{I}_{\bar{\boldsymbol{e}}})$, implying that conservativity reduction comes with an increase in computational cost. As a beneficial side effect, the degree elevation property may also lead to a relaxation of the structure imposed on the instrumental matrix $P(\boldsymbol{\vartheta})$, thereby addressing the first source of conservativity discussed at the beginning of this Section. If applying the degree elevation *after* imposing a given structure of the storage function (51), this structure will not change even if expressed as a higher degree polynomial, and the dimension of the space spanned by the allowed storage functions will remain the same. Conversely, if a new degree-elevated structure

$$P(\boldsymbol{\vartheta}) = \sum_{\boldsymbol{e} \in \mathcal{I}_{\bar{\boldsymbol{e}}}} P^{\boldsymbol{e}} \, b_{\boldsymbol{e}}^{\bar{\boldsymbol{e}}}(\boldsymbol{\vartheta}), \quad P^{\boldsymbol{e}} \in \mathbb{S}_{\bar{n}P} \; \forall \boldsymbol{e} \in \mathcal{I}_{\bar{\boldsymbol{e}}} \tag{62}$$

of total degree $\bar{\boldsymbol{e}}$ is used, all the corresponding control points $P^{\boldsymbol{e}}$ will provide independent degrees of freedom in a degree-$\bar{\boldsymbol{e}}$ expansion, therefore increasing the space of allowed storage functions enabling certification of model passivity (stability). Since polynomials converge to any arbitrary smooth multivariate function on a compact domain, this second strategy practically removes the limitations of the imposed polynomial structure on $P(\boldsymbol{\vartheta})$, as far as e is sufficiently large.

In our experiments, we observed that the degree elevation process is very effective in reducing the conservativity of the passivity constraints (54). Conversely, we did not observe relevant advantages in applying the same strategy to improve the stability constraints (40).

VII. EXPERIMENTS

We now report the results of various numerical tests of increasing complexity, in order to investigate the performance and the applicability limits of proposed approach. All experiments have been performed using a workstation equipped with 32 GB of memory and a 3.3 GHz Intel i9-X7900 CPU using a prototypal MATLAB implementation.

All tests are based on the following settings. The denominator coefficients y^{μ} are always computed by solving problem (40), while the numerator coefficients x^{μ} are estimated at the last iteration by solving problem (61) with a given level of degree elevation e. When solving this problem, we always define the structure of the matrix $P(\boldsymbol{\vartheta})$ as in (62); this implies that the number of variables involved in the problem is proportional to the number of considered constraints, i.e. $\text{Card}(\mathcal{I}_{\bar{\boldsymbol{e}}})$. The above mentioned semi-definite programs are handled via the YALMIP toolbox [39], exploiting the MOSEK interior point method for conic problems [40].

Iterations are stopped when the convergence index $\delta^{\mu} \leq 10^{-3}$; the evolution of δ^{μ} over iterations is displayed below for each test case, in order to monitor convergence based on the stabilization of denominator coefficients. With reference to a given transfer function element $\mathsf{H}^{i,j}$ and the associated

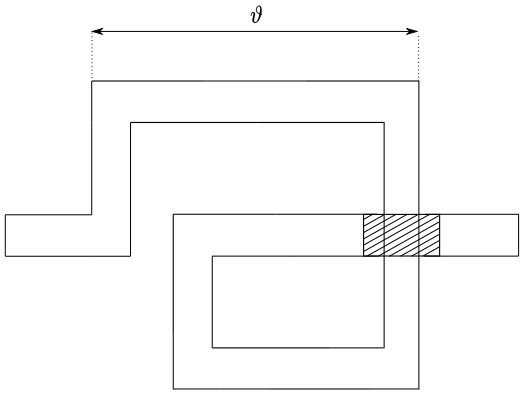

FIGURE 2. A 1.5-turn integrated inductor parameterized by the side-length $\vartheta \in [1.02, 1.52]$ mm. Drawing is not to scale.

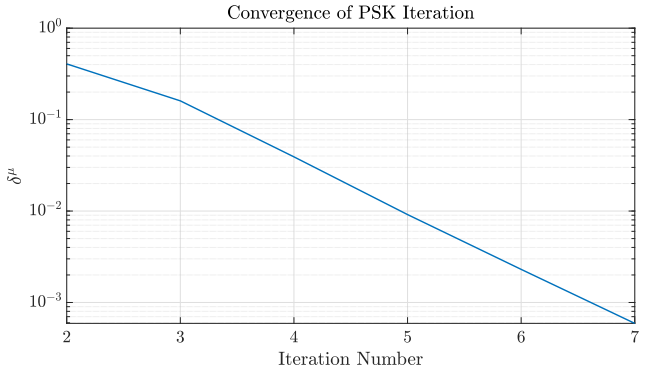

FIGURE 3. Integrated inductor. Normalized deviation of the denominator coefficients estimates, as a function of the iteration index μ.

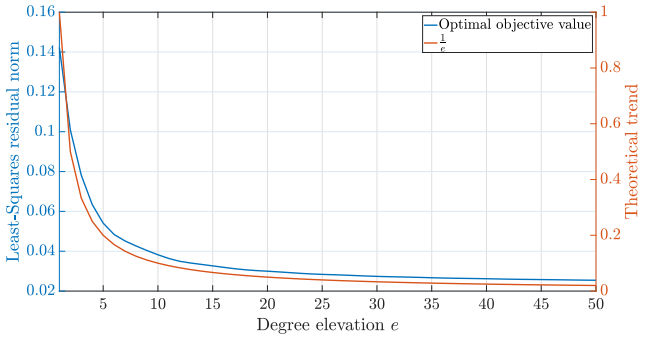

FIGURE 4. Integrated inductor. Residual norm of the constrained numerator coefficients estimation problem, as a function of the degree elevation level e. The experimental results are compared to a reference asymptotic $1/e$ trend, which is expected based on the theory [36].

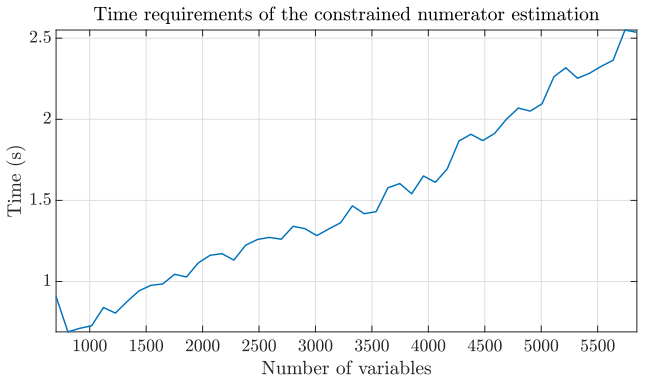

FIGURE 5. Integrated inductor. Time required to solve problem (61) as a function of the number of decision variables; the latter is directly proportional to the degree elevation e.

reference data $\tilde{H}^{i,j}$, we also define the error index

$$\epsilon_{i,j} = \max_{m=1,\dots,\bar{m}} \sqrt{\frac{1}{\bar{k}} \sum_{k=1}^{\bar{k}} \left| \frac{\mathsf{H}^{i,j}(j\omega_k, \boldsymbol{\vartheta}_m) - \tilde{H}^{i,j}_{k,m}}{\tilde{H}^{i,j}_{k,m}} \right|^2}, \quad (63)$$

which is representative of the worst case relative error of the model against the data over the design space.

In the considered datasets, the frequency-parameter spaces are sampled over logarithmically or linearly spaced grids. However, the proposed technique can be applied also in case the data are obtained according to some adaptive sampling strategy which leads to unstructured data distribution. Additionally, in some application scenarios, some a priori knowledge of the transfer function properties (e.g. degree of smoothness or resonance and anti-resonance locations) may be exploited to reduce the number $\bar{k}$ of frequency samples retrieved for each parameter configuration. This is not restrictive for the applicability of the method, provided that the data samples are sufficient to fully characterize the structure behavior.

Finally, we remark that the automated selection of the model hyper-parameters $\bar{\ell}$ and $\bar{n}$ is still an open problem. In the following examples, this selection was performed in a preprocessing stage with a basic trial and error strategy.

A. AN INTEGRATED INDUCTOR

We consider a 2-port, 1.5 turns integrated inductor, parameterized by its side-length $\boldsymbol{\vartheta} \in [1.02, 1.52]$ mm. The structure, depicted in Fig. 2, is characterized in terms of its scattering parameters in the bandwidth [0.1, 12] GHz. A total of $\bar{m} = 11$ parameter configurations are available as training data from a field solver sweep, with each dataset including $\bar{k} = 477$ logarithmically distributed frequency samples.

This training data is used to generate a passive parameterized macromodel of dynamic order $\bar{n} = 7$, using degree $\bar{\ell} = 2$ polynomials to represent the dependence of the model responses on the inductor side-length. With these settings, the solution of the semi-definite program (40) required 0.22 s on average for the 10 performed iterations. Figure 3 shows the evolution of the convergence index (19) as the iteration number increases.

At the last iteration $\mu = 7$, we solve problem (61) for different values of the degree elevation level $e = 1, \dots, 50$, in order to show the effect of the proposed conservativity reduction. Fig. 4 reports the trend of the optimal cost function resulting from the solution of (61), as a function of e. This figure confirms the effectiveness of degree elevation in the reduction of the conservativity of passivity constraints, since the residual norm of the cost function is reduced by almost one order of magnitude. The corresponding CPU time

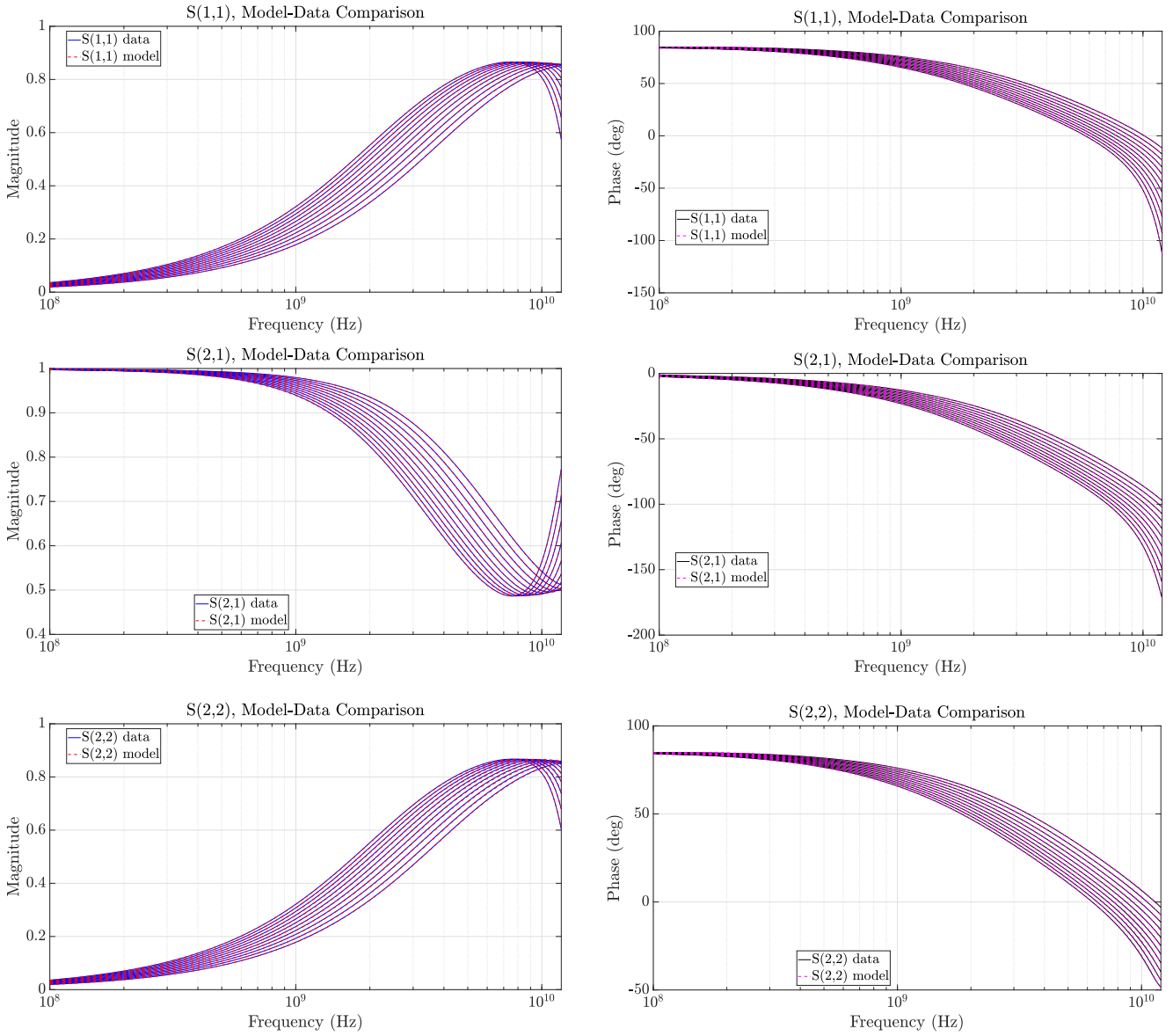

FIGURE 6. **Integrated inductor. Comparison between parameterized model responses and training data for a degree elevation level $e = 50$; all the $\bar{m} = 11$ parameter configurations are shown.**

requirements are depicted in Fig. 5, as a function of the total number of variables involved in the optimization, which in turn depends on the degree elevation order e. For this small-scale example, the computational time is modest even in the case $e = 50$, which is associated to a total of 5847 unknowns.

Considering as an example the model obtained for $e = 50$, we verified a-posteriori the non-expansivity condition 3 of the model. Therefore, we computed the model singular values over a finely sampled frequency-parameter grid, using 3000 log-spaced frequency values in the bandwidth $[0, 10^{11}]$ Hz, and 3000 linearly spaced samples in the design space. The maximum observed singular value resulted less than one, with a passivity margin $1 - \sigma_{\max} = 3 \times 10^{-10}$.

The quality of the resulting model (for the case $e = 50$) is confirmed by comparing the model responses to the training data in Fig. 6. Finally, Fig. 7 reports the relative error index $\epsilon_{2,1}$ as a function of the degree elevation e. The figure reports also the error that would be obtained by generating a model without enforcing any passivity constraint. We see that starting from $e \approx 6$ the proposed approach is able to achieve a model accuracy that is not distinguishable from the unconstrained case. We conclude that proposed framework is able to guarantee uniform model passivity by construction, with no accuracy degradation, and with limited overhead in computing time, at least for this small-scale example.

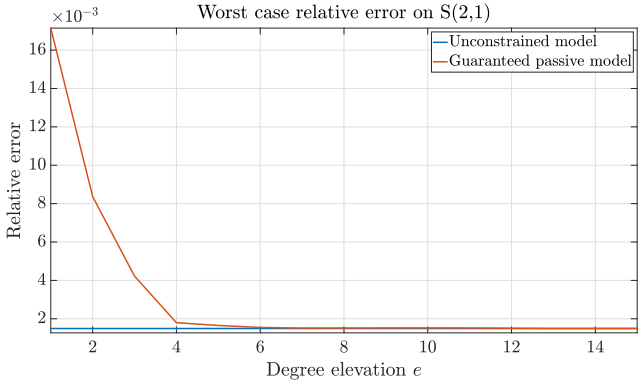

FIGURE 7. Integrated inductor. Relative error $\epsilon_{2,1}$ for different degree elevation levels e. The blue line reports the corresponding error for a model generated without enforcing any passivity constraint.

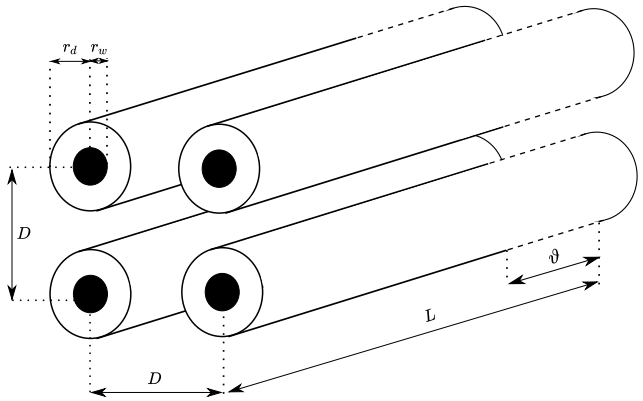

FIGURE 8. A partially-coupled multiconductor transmission line system. The parameter ϑ represents the length of the coupling. The drawing is not to scale.

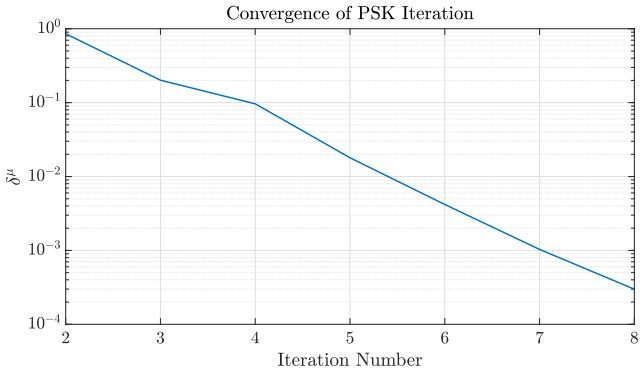

FIGURE 9. Coupled transmission line. Evolution of the convergence index δ^μ through iterations.

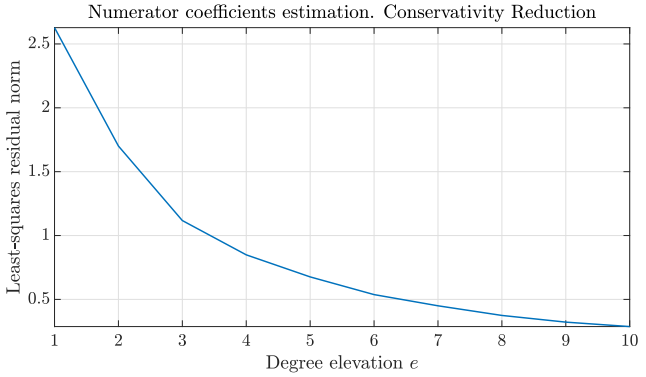

FIGURE 10. Coupled transmission line. Optimal values of the cost function in (61) for various degree elevation levels.

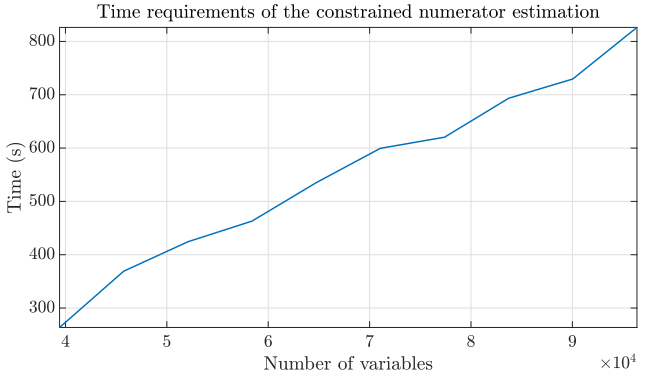

FIGURE 11. Coupled transmission line. Time required to solve problem (61) as a function of the number of decision variables corresponding to the various degree elevation levels reported in Fig. 10. The increase in the number of variables is mostly due to the increased order of the instrumental polynomial matrix $\boldsymbol{P}(\vartheta)$.

B. MULTICONDUCTOR TRANSMISSION LINE WITH VARIABLE COUPLING LENGTH

This second test case provides an academic example with a distributed coupling parameter. We consider a multiconductor transmission line with two differential pairs, each made of two equal parallel wires (radius of copper core $r_w = 0.5$ mm and dielectric coating $r_e = 0.8$ mm). The two differential pairs are placed next to each other, so that the wire centers form a square with adjacent center-to-center distance equal to 1.61 mm. The total length of the interconnect is $L = 10$ cm, but the coupling between the two pairs in the corresponding per-unit-length matrices is considered only over a portion of the length $L_c = \vartheta \in \Theta = [20, 40]$ mm, which is the independent parameter considered for this study. The lines are considered as uncoupled for the remaining length $L - L_c$. Figure 8 provides a graphical description for the structure. This example is selected to illustrate the shifting of the resonances as ϑ changes, and the capability of the model to track such resonances (the parameterized model poles) thanks to the adopted model structure.

The design space is sampled with $\bar{m} = 11$ linearly spaced values. For each parameter configuration a total of $\bar{k} = 499$ logarithmically spaced frequency samples of the 4×4 scattering matrix are extracted in the bandwidth $[0.01, 5]$ GHz. These samples are used to generate a model of dynamic order $\bar{n} = 28$, whereas numerator $\mathsf{N}(s, \boldsymbol{\vartheta})$ and denominator $\mathsf{D}(s, \boldsymbol{\vartheta})$ are parameterized by Bernstein polynomials of order 4 and 2, respectively.

The convergence of the identification algorithm is demonstrated in Fig. 9, where the value of δ^μ for $\mu \geq 1$ is reported. For this example, we built 10 different models,

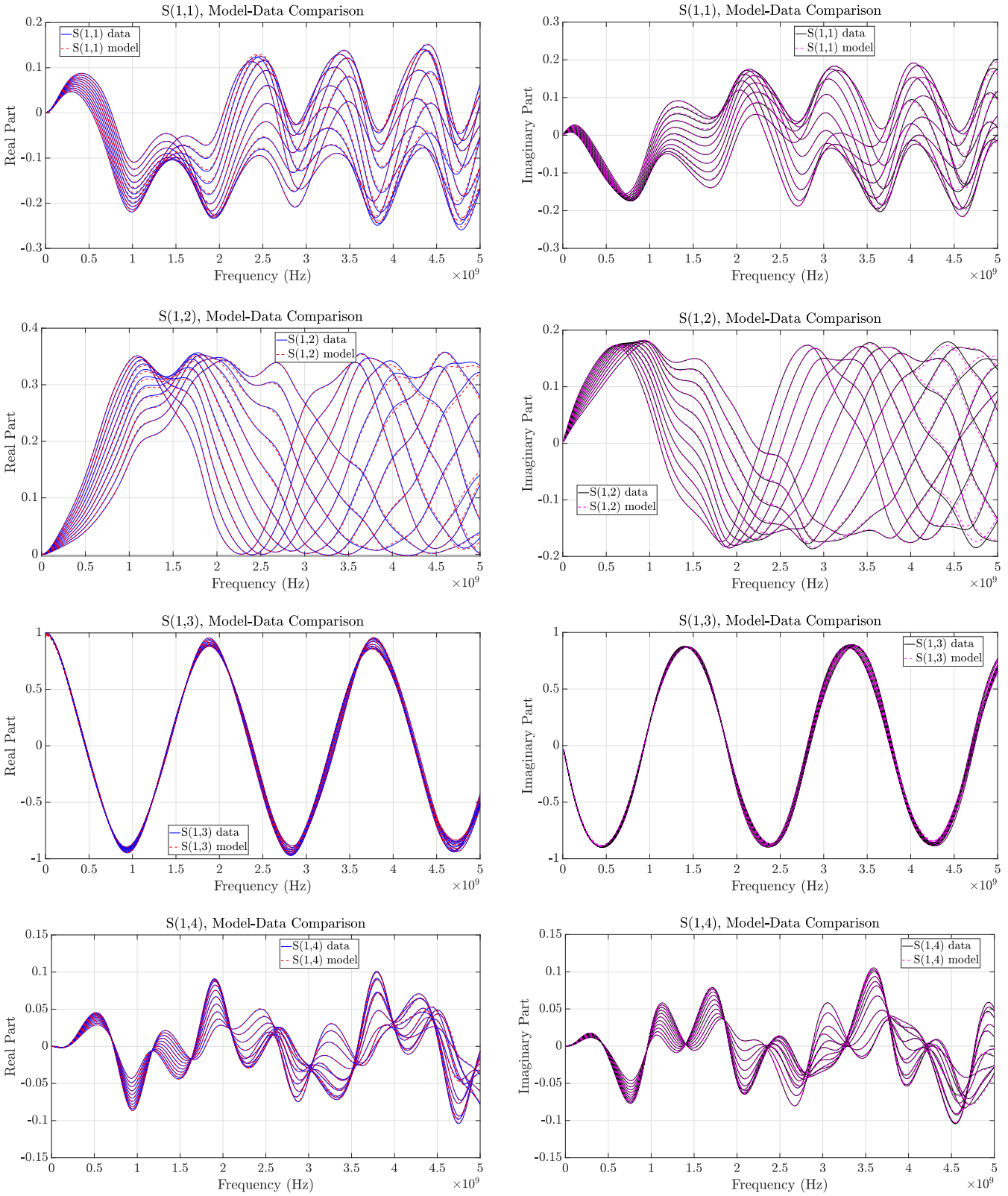

FIGURE 12. Coupled transmission line. Fitting results for the first-column of the transfer matrix. The elements that are not shown here exhibit similar trends and a comparable model accuracy.

solving each time problem (61) with different levels of degree elevation $e = 1, 2, \ldots, 10$. Figure 10 reports the optimal cost function value from the solution of problem (61) for different degree elevation levels e. The average time required to solve

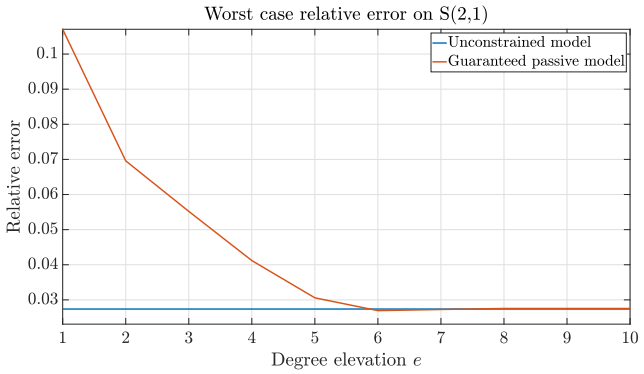

FIGURE 13. Coupled transmission line. Relative error $\epsilon_{2,1}$ for the passive models based on different degree elevations, compared to the error of the model obtained without enforcing any passivity constraint.

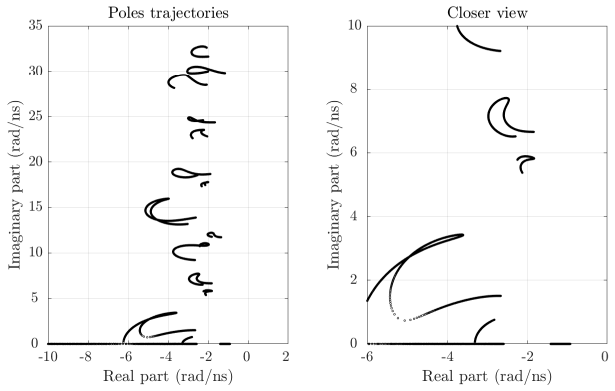

FIGURE 14. Parameterized poles trajectories of the coupled transmission line model. Left panel: in-band poles. Right panel: enlarged view on the low-frequency region.

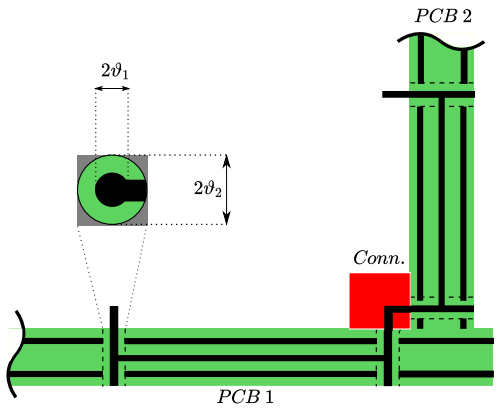

FIGURE 15. High-speed PCB stripline interconnect parameterized by via pad and antipad radii. Drawing for illustration only and not to scale.

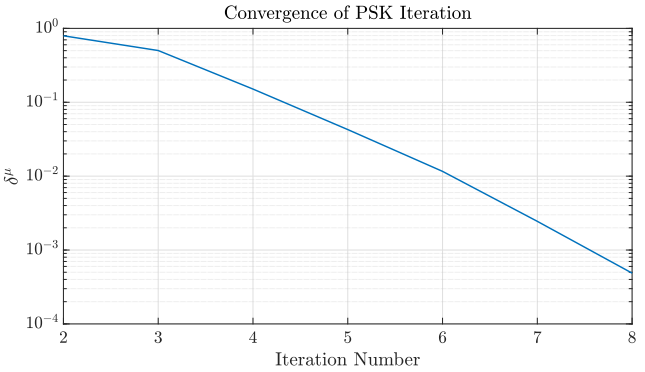

FIGURE 16. High-speed link. Convergence of denominator coefficients estimates through iterations.

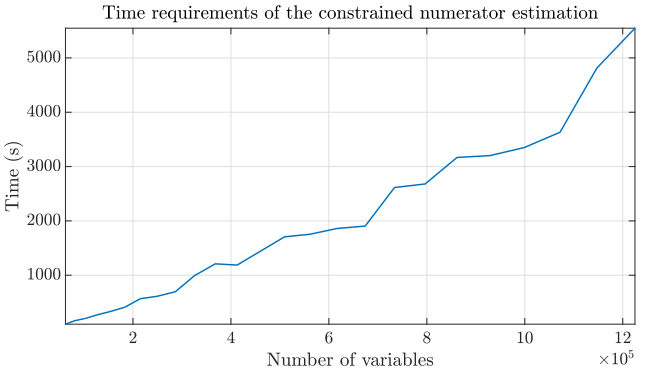

FIGURE 17. High-speed link. Time required to enforce the model passivity, as a function of the number of variables required by different degree elevation levels.

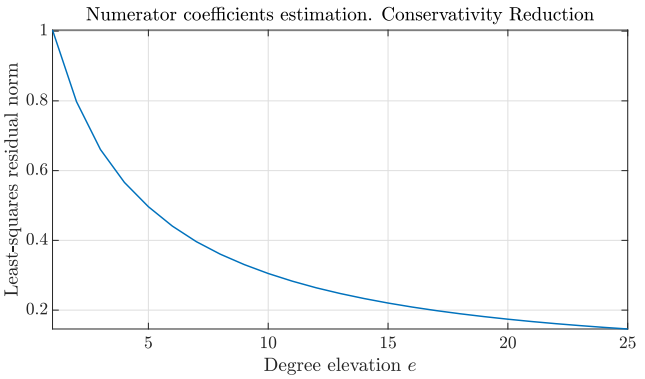

FIGURE 18. High-speed link. Cost function reduction for increasing degree elevation during passivity enforcement.

problem (40) is 0.72 s, while the time required to solve (61) depends on the degree elevation level. The actual runtimes for this test case are reported in Fig. 11.

Figure 12 reports the modeling results obtained with $e = 10$ for the entire first column of the scattering matrix, while Fig. 13 depicts the model relative error $\epsilon_{2,1}$ as a function of the degree elevation e. These results confirm that also for this case the error approaches the limit corresponding to the unconstrained (hence not guaranteed passive) model, computed using the same training dataset. A graphical representation of the model parameterized poles trajectories is given in Fig 14, computed over a very fine sweep of the free parameter $\vartheta \in \Theta$. As expected, all the poles are stable with a negative real part, uniformly in the parameter space. The presence of bifurcations further confirms the effectiveness of the proposed approach in modeling non-smooth poles

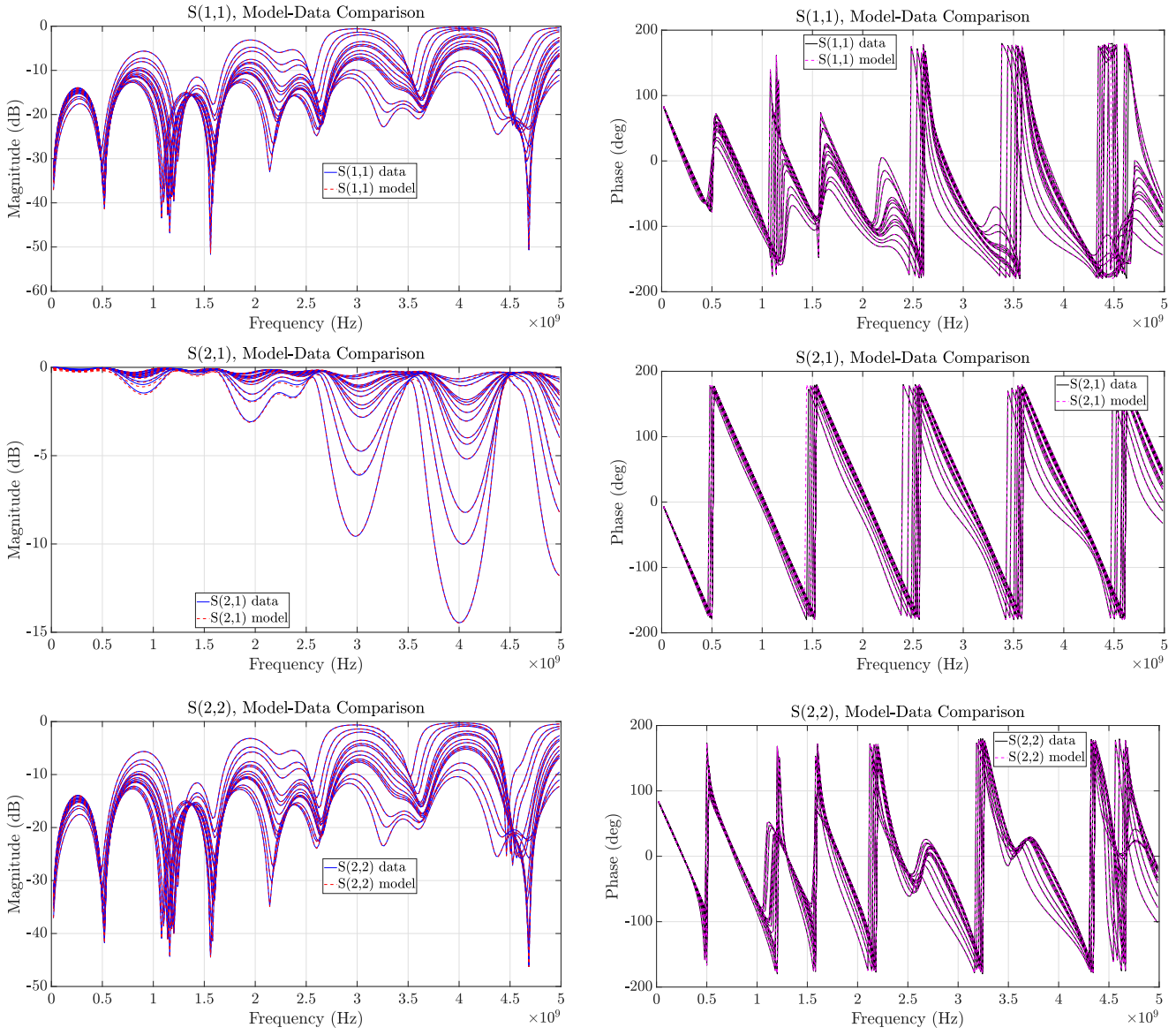

FIGURE 19. High-speed link. Comparison of model responses ($e = 25$) with the corresponding raw data over a random subset of 14 out of the total 81 available frequency responses.

behaviors, thanks to the implicit parameterization provided by the adopted model structure.

C. A TWO-PARAMETER HIGH-SPEED PCB LINK

This test case considers a 2-parameter structure, namely a high-speed stripline link running through two PCBs attached by a connector and the corresponding via fields, first presented in [41]. A schematic layout of the structure is depicted in Fig. 15. The PCB substrate has permittivity $\epsilon_r = 3$ and $\tan\delta = 0.002$. The vertical vias are parameterized by the pad radius $\vartheta_1 \in [100, 300]$ μm and the associated antipad radius $\vartheta_2 \in [400, 600]$ μm. See [41] for full details.

The scattering parameters of the structure are available from a field solver (courtesy of Prof. Schuster, TUHH, Germany) at $\bar{k} = 250$ frequency points linearly spaced in the interval $[0.02, 5]$ GHz, and over a 9×9 uniform grid in the parameter space. These data are used to generate a parameterized macromodel with $\bar{n} = 25$ poles and polynomial order of numerator and denominator $\bar{\ell} = (3, 2)$.

The convergence of the denominator coefficient estimation is illustrated by plotting δ^{μ} in Fig. 16. With the considered model structure, the time required to solve (40), averaged over the 8 PSK iterations amounts to 1.5 s. For this example, we considered a number of possible degree elevations levels e ranging from 1 to 25. The time required to build each of the 25 models is depicted in Fig. 17. We observe that, although the time requirements for this example are larger, the solver scales favourably with the increase in the number of instrumental variables induced by the higher degree elevations (almost linearly, at least up to 10^5 variables).

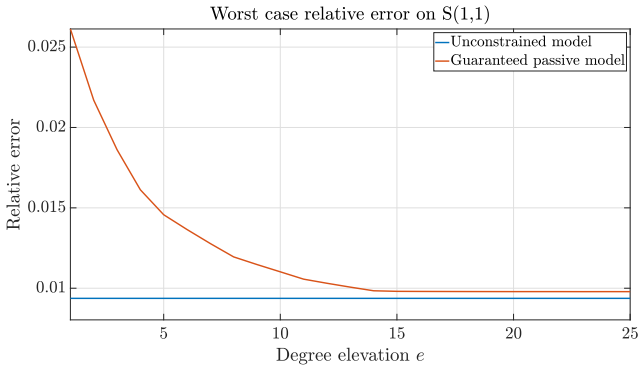

FIGURE 20. High-speed link. Evolution of the relative error $\epsilon_{1,1}$ for the passive models with different degree elevations, compared to the unconstrained model error.

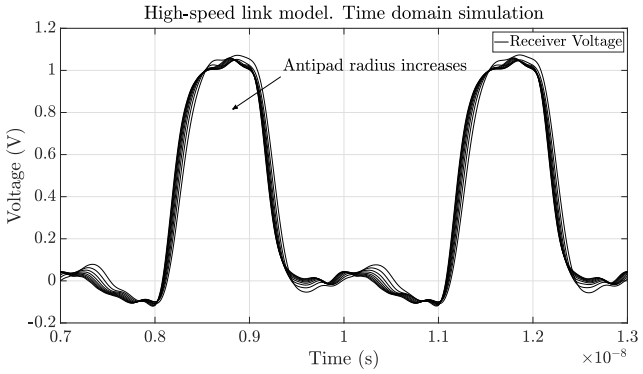

FIGURE 21. Parameterized transient analysis of the high-speed link equivalent circuit. The simulation is performed by considering eight different antipad radius configurations in the interval [400, 600]μm, while keeping fixed the pad radius to 300μm. Two periods of the output signal are shown.

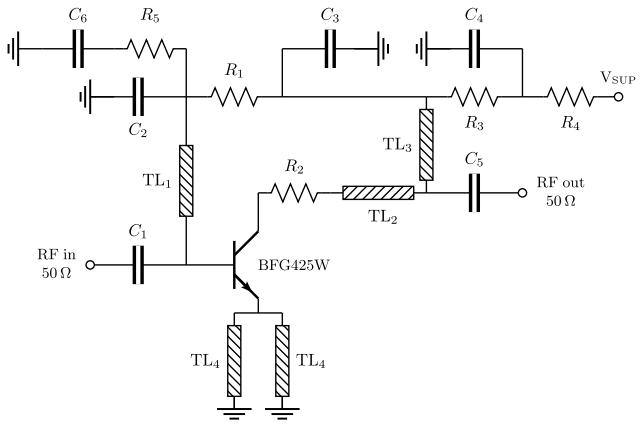

FIGURE 22. The LNA circuit schematic.

The value of the optimal cost function value of the semi-definite program (55) for different values of e is reported in Fig. 18, and confirms the same decreasing trend that has been observed in single-parameter test cases.

For the case $e = 25$, a visual comparison between the parameterized model frequency response and the reference data is provided in Fig. 19, considering a subset of 14 random parameter configurations out of the available 81. Also in this case, the accuracy of the model is remarkable throughout the considered frequency band, with no visual difference between model and data on this scale. Finally, Fig. 20 reports the relative error $\epsilon_{1,1}$ for different degree elevations. Also for this case the error stabilizes to the same error of the unconstrained (non-passive) model; this occurs at about $e = 15$.

In order to assess the influence of the design parameters on the time-domain responses, and to demonstrate the efficiency of the parameterized models in a typical use case scenario, we performed a transient simulation of the equivalent parameterized SPICE circuit synthesized from the model. The simulation setup includes a 50Ω voltage driver launching a pulse sequence with amplitude 1 V, period $T = 3$ ns, rise and fall time 200 ps, and bit duration 0.8 ns. The receiver side is instead terminated by a RC parallel load, with $R = 1$ kΩ and $C = 2$ pF. We considered a fixed pad radius $\vartheta_1 = 300$ μm, and we let the antipad radius vary, by considering a linear sweep of 8 configurations within its allowed range. The results of the simulation are depicted in Fig. 21, where the voltage signals at the receiver are shown. The time requirements of each simulation amounted to 0.5 s using a freeware SPICE solver.

D. AN ACTIVE DEVICE

In this last example we generate a reduced-order small-signal model of the Low Noise Amplifier (LNA) depicted in Fig. 22, which includes both lumped elements and lossy transmission lines. The circuit depends on $d = 7$ design parameters, which are listed in Table 1. The device was first presented in [42]; additionally, it was considered as a test-bench for the generation of uniformly stable parameterized macromodels in [24].

The purpose of this test case is two-fold. First, we show that even in case of high-dimensional design spaces, the generation of uniformly stable parameterized macromodels can be efficiently tackled by solving problem (40). Second, we show how the proposed approach is less conservative than the current state-of-the-art method [24] providing a formal guarantee of uniform stability given model structure (13). Of course, uniform passivity is not applicable since this is an active device.

We consider a fixed operating point $V_{SUP} = 4.5$ V and we construct a small-signal linearized model. A total of $\bar{m} = 1400$ parameter configurations are considered according to a latin-hypercube distribution in the design space. For each fixed configuration, the reflection coefficient at the amplifier input port is sampled at $\bar{k} = 701$ logarithmically spaced frequency points in the interval [1, 10] GHz. Only 595 parameter configurations are exploited to generate a parameterized macromodel with $\bar{n} = 10$ and $\bar{\ell} = (1, 1, 1, 1, 1, 1, 2)$, while the remaining samples are left for model validation.

With this configuration, the modeling algorithm reaches the stopping threshold $\delta^{\mu} = 10^{-3}$ in only 3 iterations. The

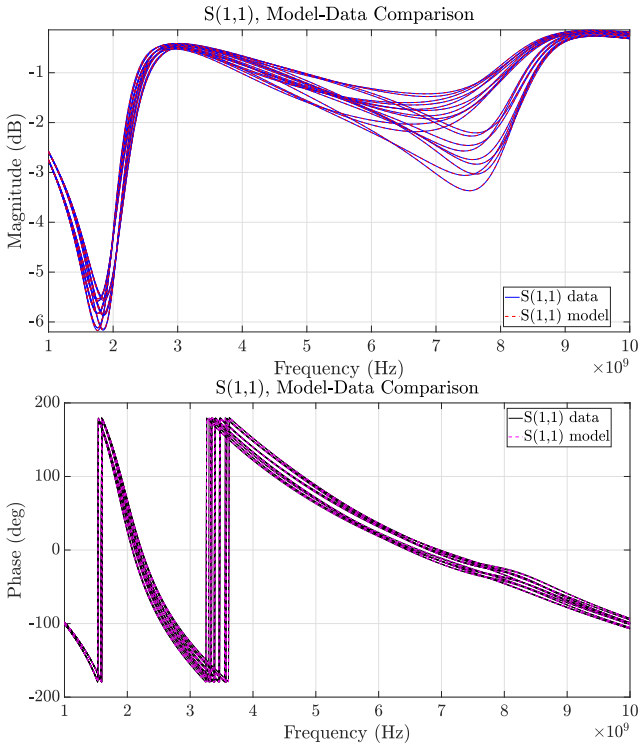

FIGURE 23. LNA example. Comparison between model responses and validation data over 19 different frequency responses, randomly selected in the design space.

TABLE 1. Free parameters considered for the modeling of the LNA test case. First six parameters: parasitic inductances and capacitances of the transistor. Parameter h is the substrate thickness for lines TL_1, TL_2, TL_3.

#	Parameter ϑ_i	$\vartheta_{i,\min}$	$\vartheta_{i,\max}$
1	L_b (nH)	0.88	1.32
2	L_c (nH)	0.88	1.32
3	L_e (nH)	0.20	0.30
4	C_{cb} (pF)	0.0016	0.0024
5	C_{be} (pF)	0.064	0.096
6	C_{ce} (pF)	0.064	0.096
7	h (mm)	0.45	0.55

average time to solve (40) is 6 s, and the relative error index results $\epsilon = 1.42 \times 10^{-3}$, confirming that the model is highly accurate also in correspondence of the validation samples. In Fig. 23, we provide a visual comparison between the model and the data, for 19 different randomly-selected validation responses.

In order to show the low degree of conservativity of the proposed stability constraints, we repeated the same experiment performed in [24], where the uniform stability is enforced by imposing a sign inequality directly on the denominator coefficients $r_{n,\ell}$ during the model generation. For this purpose, we considered the same LNA device and restricted the dimension of the design space to $d = 5$, by taking into account only the first five parameters listed in Table 1. We built a model by setting $\bar{n} = 16$ and $\bar{\boldsymbol{\ell}} = (1, 1, 1, 1, 1)$, as in the referenced article.

The stop criterion $\delta^{\mu} = 10^{-3}$ was met after 4 iterations, with an average computing time required to solve (40) equal to 1.2 s. We computed the relative error index of the resulting model, obtaining $\epsilon = 6.36 \times 10^{-5}$; the same index for a model based on [24] was $\epsilon = 1.94 \times 10^{-2}$. Thus, the proposed technique provides a decrease of the worst case relative error of about 3 orders of magnitude, while guaranteeing the uniform model stability by construction. This improvement is attained in approximately the same runtime.

VIII. CONCLUSION

This work presented a passive macromodeling strategy that can be successfully used to generate surrogates of small-to-medium size passive multiport structures characterized by a limited number of degrees of freedom. The approach combines the desirable model compactness feature, typical of approaches based on multivariate rational fitting, with the theoretical warranty of uniform model passivity throughout the design space. As a particular case, removing passivity conditions enables parameterized (linearized small-signal) macromodeling of active devices with uniform stability constraints.

The proposed stability and passivity constraints are conservative since based on a discretization of continuous positive and/or bounded realness conditions in a multidimensional parameter space. However, the amount of the conservativity in the stability and passivity constraints can be effectively controlled in terms of the Bernstein polynomial degree elevation, which provides an algorithm control knob. Therefore, the proposed method naturally allows users to select the most appropriate trade-off between computational time requirements for the model extraction and model accuracy.

Various numerical examples show that stability enforcement is attained in seconds for typical small-medium scale problems, whereas passivity enforcement requires a larger runtime, which depends on the cumulative number of decision variables. The latter depends on the number of model poles, the degree of polynomials providing model parameterization, as well as the number of instrumental variables that are required to cast the proposed constraints in a convex form. Future research directions will be devoted to the reduction of the computational burden required by the proposed strategy, with the objective of handling larger and more complex electrical, electronic or electromagnetic structures, and/or the concurrent dependence on more free parameters.

REFERENCES

[1] T. Zhang, K. Chakrabarty, and R. B. Fair, "Behavioral modeling and performance evaluation of microelectrofluidics-based PCR systems using SystemC," *IEEE Trans. Comput.-Aided Design Integr.*, vol. 23, no. 6, pp. 843–858, Jun. 2004.

[2] G. Casinovi and A. Sangiovanni-Vincentelli, "A macromodeling algorithm for analog circuits," *IEEE Trans. Comput.-Aided Design Integr. Circuits Syst.*, vol. 10, no. 2, pp. 150–160, Feb. 1991.

[3] I. S. Stievano, I. A. Maio, and F. G. Canavero, "Parametric macromodels of digital I/O ports," *IEEE Trans. Adv. Packag.*, vol. 25, no. 2, pp. 255–264, May 2002.

[4] G. Antonini, D. Deschrijver, and T. Dhaene, "Broadband rational macromodeling based on the adaptive frequency sampling algorithm and the partial element equivalent circuit method," *IEEE Trans. Electromagn. Compat.*, vol. 50, no. 1, pp. 128–137, Feb. 2008.

[5] R. Araneo, "Extraction of broad-band passive lumped equivalent circuits of microwave discontinuities," *IEEE Trans. Microw. Theory Techn.*, vol. 54, no. 1, pp. 393–401, Jan. 2006.

[6] S. Grivet-Talocia and B. Gustavsen, *Passive Macromodeling: Theory and Applications*, vol. 239. Hoboken, NJ, USA: Wiley, 2015.

[7] B. Gustavsen and A. Semlyen, "Rational approximation of frequency domain responses by vector fitting," *IEEE Trans. Power Del.*, vol. 14, no. 3, pp. 1052–1061, Jul. 1999.

[8] Y. Nakatsukasa, O. Sète, and L. N. Trefethen, "The AAA algorithm for rational approximation," *SIAM J. Sci. Comput.*, vol. 40, no. 3, pp. A1494–A1522, Jan. 2018.

[9] M. Berljafa and S. Güttel, "Generalized rational Krylov decompositions with an application to rational approximation," *SIAM J. Matrix Anal. Appl.*, vol. 36, no. 2, pp. 894–916, 2015.

[10] S. Lefteriu and A. C. Antoulas, "A new approach to modeling multiport systems from frequency-domain data," *IEEE Trans. Comput.-Aided Design Integr. Circuits Syst.*, vol. 29, no. 1, pp. 14–27, Jan. 2010.

[11] E. R. Samuel, L. Knockaert, F. Ferranti, and T. Dhaene, "Guaranteed passive parameterized macromodeling by using Sylvester state-space realizations," *IEEE Trans. Microw. Theory Techn.*, vol. 61, no. 4, pp. 1444–1454, Apr. 2013.

[12] F. Ferranti, L. Knockaert, and T. Dhaene, "Parameterized S-parameter based macromodeling with guaranteed passivity," *IEEE Microw. Wireless Compon. Lett.*, vol. 19, no. 10, pp. 608–610, Oct. 2009.

[13] A. C. Rodriguez and S. Gugercin, "The p-AAA algorithm for data driven modeling of parametric dynamical systems," 2020, *arXiv:2003.06536*.

[14] P. Triverio, S. Grivet-Talocia, and M. S. Nakhla, "A parameterized macromodeling strategy with uniform stability test," *IEEE Trans. Adv. Packag.*, vol. 32, no. 1, pp. 205–215, Feb. 2009.

[15] Y. Q. Xiao, S. Grivet-Talocia, P. Manfredi, and R. Khazaka, "A novel framework for parametric Loewner matrix interpolation," *IEEE Trans. Compon., Packag., Manuf. Technol.*, vol. 9, no. 12, pp. 2404–2417, Dec. 2019.

[16] S. Grivet-Talocia, "On driving non-passive macromodels to instability," *Int. J. Circuit Theory Appl.*, vol. 37, no. 8, pp. 863–886, Oct. 2009.

[17] S. Grivet-Talocia, "Passivity enforcement via perturbation of Hamiltonian matrices," *IEEE Trans. Circuits Syst. I, Reg. Papers*, vol. 51, no. 9, pp. 1755–1769, Sep. 2004.

[18] D. Deschrijver and T. Dhaene, "Fast passivity enforcement of *S*-parameter macromodels by pole perturbation," *IEEE Trans. Microw. Theory Techn.*, vol. 57, no. 3, pp. 620–626, Mar. 2009.

[19] S. Grivet-Talocia and A. Ubolli, "On the generation of large passive macromodels for complex interconnect structures," *IEEE Trans. Adv. Packag.*, vol. 29, no. 1, pp. 39–54, Feb. 2006.

[20] F. Ferranti, L. Knockaert, T. Dhaene, and G. Antonini, "Passivity-preserving parametric macromodeling for highly dynamic tabulated data based on lur'e equations," *IEEE Trans. Microw. Theory Techn.*, vol. 58, no. 12, pp. 3688–3696, Dec. 2010.

[21] F. Ferranti, L. Knockaert, and T. Dhaene, "Passivity-preserving parametric macromodeling by means of scaled and shifted state-space systems," *IEEE Trans. Microw. Theory Techn.*, vol. 59, no. 10, pp. 2394–2403, Oct. 2011.

[22] S. Grivet-Talocia, "A perturbation scheme for passivity verification and enforcement of parameterized macromodels," *IEEE Trans. Compon., Packag., Manuf. Technol.*, vol. 7, no. 11, pp. 1869–1881, Nov. 2017.

[23] S. Grivet-Talocia and R. Trinchero, "Behavioral, parameterized, and broadband modeling of wired interconnects with internal discontinuities," *IEEE Trans. Electromagn. Compat.*, vol. 60, no. 1, pp. 77–85, Feb. 2018.

[24] A. Zanco, S. Grivet-Talocia, T. Bradde, and M. De Stefano, "Uniformly stable parameterized macromodeling through positive definite basis functions," *IEEE Trans. Compon., Packag., Manuf. Technol.*, vol. 10, no. 11, pp. 1782–1794, Nov. 2020.

[25] A. Zanco, S. Grivet-Talocia, T. Bradde, and M. De Stefano, "Enforcing passivity of parameterized LTI macromodels via Hamiltonian-driven multivariate adaptive sampling," *IEEE Trans. Comput.-Aided Design Integr. Circuits Syst.*, vol. 39, no. 1, pp. 225–238, Jan. 2020.

[26] T. Bradde, A. Zanco, and S. Grivet-Talocia, "Bivariate macromodeling with passivity constraints," in *Proc. IEEE 30th Conf. Electr. Perform. Electron. Packag. Syst. (EPEPS)*, Oct. 2021, pp. 1–3.

[27] A. Kojima, "A characterization of parameter-dependent LMIs on Bernstein polynomial basis," in *Proc. IEEE Conf. Decis. Control (CDC)*, Dec. 2018, pp. 4687–4694.

[28] J. Berchtold and A. Bowyer, "Robust arithmetic for multivariate bernstein-form polynomials," *Comput.-Aided Des.*, vol. 32, no. 11, pp. 681–689, Sep. 2000.

[29] A. Zanco and S. Grivet-Talocia, "Toward fully automated high-dimensional parameterized macromodeling," *IEEE Trans. Compon., Packag., Manuf. Technol.*, vol. 11, no. 9, pp. 1402–1416, Sep. 2021.

[30] B. Gustavsen, "Improving the pole relocating properties of vector fitting," in *Proc. IEEE Power Eng. Soc. Gen. Meeting*, Jun. 2006, p. 1.

[31] T. Bradde, S. Grivet-Talocia, M. De Stefano, and A. Zanco, "A scalable reduced-order modeling algorithm for the construction of parameterized interconnect macromodels from scattering responses," in *Proc. IEEE Symp. Electromagn. Compat., Signal Integrity Power Integrity (EMC, SI PI)*, Jul. 2018, pp. 650–655.

[32] M. R. Wohlers, *Lumped and Distributed Passive Networks*. New York, NY, USA: Academic, 1969.

[33] S. V. Gusev and A. L. Likhtarnikov, "Kalman-Popov-Yakubovich lemma and the S-procedure: A historical essay," *Autom. Remote Control*, vol. 67, no. 11, pp. 1768–1810, Nov. 2006.

[34] L. Vandenberghe, V. R. Balakrishnan, R. Wallin, A. Hansson, and T. Roh, "Interior-point algorithms for semidefinite programming problems derived from the KYP lemma," in *Positive Polynomials Control*. Berlin, Germany: Springer, 2005, pp. 195–238.

[35] B. D. Anderson and S. Vongpanitlerd, *Network Analysis and Synthesis: A Modern Systems Theory Approach*. New York, NY, USA: Dover, 2013.

[36] F. J. Li, "Interpolation and convergence of Bernstein–Bézier coefficients," *Acta Math. Sinica, English Ser.*, vol. 27, no. 9, p. 1769, 2011.

[37] G. Farin, *Curves and Surfaces for Computer-Aided Geometric Design: A Practical Guide*. Amsterdam, The Netherlands: Elsevier, 2014.

[38] H. Prautzsch and L. Kobbelt, "Convergence of subdivision and degree elevation," *Adv. Comput. Math.*, vol. 2, no. 1, pp. 143–154, Jan. 1994.

[39] J. Lofberg, "YALMIP : A toolbox for modeling and optimization in MATLAB," in *Proc. IEEE Int. Conf. Robot. Autom.*, Sep. 2004, pp. 284–289.

[40] M. ApS. (2021). *MOSEK Optimizer API for C*. [Online]. Available: https://docs.mosek.com/9.3/capi.pdf

[41] J. Preibisch, T. Reuschel, K. Scharff, J. Balachandran, B. Sen, and C. Schuster, "Exploring efficient variability-aware analysis method for high-speed digital link design using PCE," in *Proc. DesignCon*, 2017, pp. 1–19.

[42] T. Buss, "2GHz low noise amplifier with the BFG425W," Philips Semicond., Nijmegen, The Netherlands, Tech. Rep. RNR-T45-96-B-773, 1996. [Online]. Available: http://application-notes.digchip.com/004/4-7999.pdf

TOMMASO BRADDE (Member, IEEE) received the bachelor's degree in electronic engineering from Roma Tre University, Rome, Italy, in 2015, and the master's degree in mechatronic engineering, Politecnico di Torino, Turin, Italy, in 2018, where he is currently pursuing the Ph.D. degree in electrical, electronics and communication engineering. His research interests include data-driven parameterized macromodeling and its applications to system level signal and power integrity assessments, with the inclusion of active devices. He was a co-recipient of the 2018 Best Paper Award of the IEEE International Symposium on Electromagnetic Compatibility, the 2020 Best Paper Award of the IEEE Conference on Electrical Performance of Electronic Packaging and Systems (EPEPS), the Best Student Paper Award of the 23rd IEEE Workshop on Signal and Power Integrity, and the Best Student Paper Award of the 2021 EPEPS Symposium.

STEFANO GRIVET-TALOCIA (Fellow, IEEE) received the Laurea and Ph.D. degrees in electronic engineering from the Politecnico di Torino, Turin, Italy. From 1994 to 1996, he was with the NASA/Goddard Space Flight Center, Greenbelt, MD, USA. He is currently a Full Professor of electrical engineering with the Politecnico di Torino. He co-founded the academic spinoff company IdemWorks, Turin, in 2007, where he served as the President until its acquisition by CST, in 2016. He has authored about 200 journals and conference papers. His current research interests include passive macromodeling of lumped and distributed interconnect structures, model-order reduction, modeling and simulation of fields, circuits, and their interaction, wavelets, time-frequency transforms, and their applications. He was a co-recipient of the 2007 Best Paper Award of the IEEE TRANSACTIONS ON ADVANCED PACKAGING. He received the IBM Shared University Research Award in 2007, 2008, and 2009. He was the General Chair of the 20th and 21st IEEE Workshops on Signal and Power Integrity (SPI2016 and SPI2017). He is currently the Chair of the Technical Committee on Electrical Design, Modeling and Simulation, IEEE Electronic Packaging Society. He was an Associate Editor of the IEEE TRANSACTIONS ON ELECTROMAGNETIC COMPATIBILITY, from 1999 to 2001. He is currently serving as an Associate Editor for the IEEE TRANSACTIONS ON COMPONENTS, PACKAGING AND MANUFACTURING TECHNOLOGY.

ALESSANDRO ZANCO (Member, IEEE) received the bachelor's degree in electrical engineering and the master's degree in mechathronic engineering from the Politecnico di Torino, Torino, Italy, in 2015 and 2018, respectively, where he is currently pursuing the Ph.D. degree in electrical, electronics and communication engineering. His research interest includes high-dimensional parameterized black-box modeling for EMC.

GIUSEPPE C. CALAFIORE (Fellow, IEEE) received the master's degree in financial data science from the University of California, Berkeley. He held visiting positions at the Information Systems Laboratory (ISL), Stanford University, California, in 1995; the Ecole Nationale Supérieure de Techniques Avancées (ENSTA), Paris, in 1998; and the University of California, in 1999, 2003, 2007, 2017, 2018, and 2019. He was a Senior Fellow with the Institute of Pure and Applied Mathematics (IPAM), University of California, Los Angeles, in 2010. He is currently a Full Professor with DET, Politecnico di Torino, where he coordinates the Control Systems and Data Science Group and an Associate Fellow of IEIIT-CNR. He has over 20 years of teaching experience in master-level and Ph.D. courses in the areas of systems and control theory, convex optimization and machine learning. He is the author of about 200 journals and conference proceedings papers and eight books. His research interests include convex optimization, identification and control of uncertain systems, with applications ranging from finance and economic systems to robust control, machine learning, and data science. He received the IEEE Control System Society "George S. Axelby" Outstanding Paper Award, in 2008.